Quantifying Molecular Mixing and Heterogeneity in Pharmaceutical Dispersions at Sub-100-nm Resolution by Spin Diffusion NMR

Pu Duan¹, Matthew S. Lamm², Fengyuan Yang², Wei Xu², Daniel Skomski², Yongchao Su^{2,3,4*}, and Klaus Schmidt-Rohr^{1,*}

Submitted to *Molecular Pharmaceutics*

Revised July 2020

¹ Department of Chemistry, Brandeis University, Waltham, Massachusetts 02453, United States

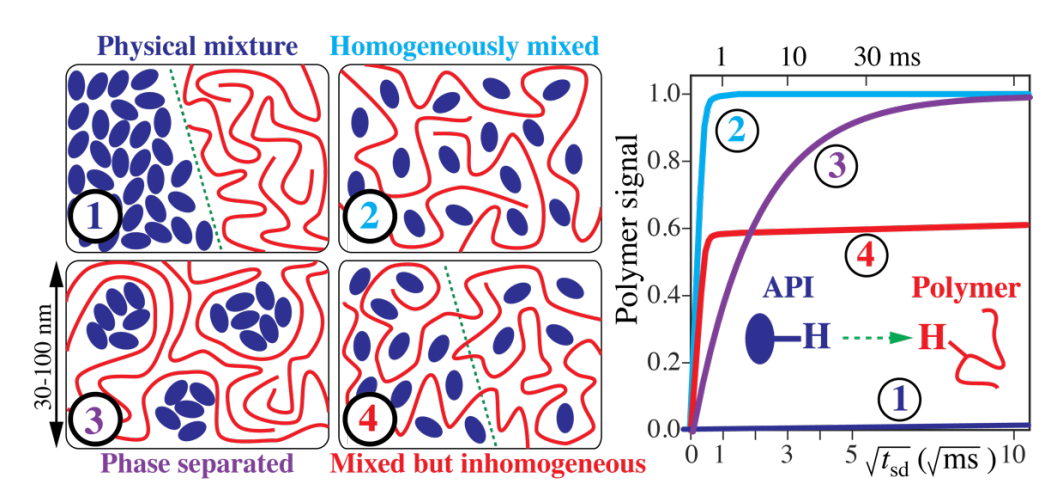
² Pharmaceutical Sciences, Merck & Co., Inc., Kenilworth, New Jersey 07033, United States

³ Department of Industrial and Physical Pharmacy, College of Pharmacy, Purdue University, Indiana 47907, United States

⁴ Division of Molecular Pharmaceutics and Drug Delivery, College of Pharmacy, The University of Texas at Austin, Austin, Texas 78712, United States

^{*} Corresponding authors: K.S.R.: srohr@brandeis.edu and Y.S.: yongchao.su@merck.com

Table of Content Figure



Abstract

Molecular miscibility and homogeneity of amorphous solid dispersions (ASDs) are critical attributes that impact physiochemical stability, bioavailability and processability. Observation of a single glass transition is utilized as a criterion for good mixing of drug substance and polymeric components but can be misleading and cannot quantitatively analyze the domain size at high resolution. While imaging techniques, on the other hand, can characterize phase separation on the particle surface at the nanometer scale, they often require customized sample preparation and handling. Moreover, a mixed system is not necessarily homogeneous. Compared to the numerous studies that have evaluated the mixing of drug substance and polymer in ASDs, inhomogeneity in the phase compositions has remained significantly underexplored. To overcome the analytical challenge, we have developed a ¹H spin diffusion NMR technique to quantify molecular mixing of bulk ASDs at sub-100-nm resolution. It combines relaxation filtering $(T_{2,H})$ and T_{1p}) that leaves the active pharmaceutical ingredient (API) as the main source of ¹H magnetization at the start of spin diffusion to the polymer matrix. A spray-dried nifedipinepolyvinylpyrrolidone (Nif-PVP) ASD at 5 wt% drug loading was a homogeneous reference system that exhibited equilibration of magnetization transfer from API to polymer within a short spin diffusion time of 3 ms. While fast initial magnetization transfer proving mixing on the 1-nm scale was also observed in Nif-PVP ASDs prepared by hot-melt extrusion (HME) at 186 °C at 40 wt% drug loading, incomplete equilibration of peak intensities documented inhomogeneity on the ≥30 nm scale. The nonuniformity was confirmed by partial inversion of the Nif magnetization in the filter that resulted in an even more pronounced deviation from equilibration, and by ¹H-¹³C heteronuclear correlation (HETCOR) NMR. It is consistent with the observed differential ¹H spin-lattice relaxation of Nif and PVP as well as a domain structure on the 20-nm scale observed in AFM images. The incomplete equilibration and differential relaxation were consistently reproduced in a model of two mixed phases of different compositions, e.g. 40 wt% of the ASD with 15 wt% drug loading and the remaining 60 wt% with 56 wt% drug loading. Hot melt extrusion produced more inhomogeneous samples than spray drying for the samples examined in our study. To the best of our knowledge, this spin diffusion NMR method provides currently the highest resolution quantification of inhomogeneous molecular mixing and phase composition in bulk samples of pharmaceutical dispersions produced with equipment, procedures, and drug loadings that are relevant to industrial drug development.

Keywords: Amorphous solid dispersion; miscibility and homogeneity; phase separation; NMR relaxation; spin diffusion NMR

1. Introduction

Aqueous solubility of a drug is one of the most fundamental attributes during drug development, as it significantly impacts oral bioavailability. Low aqueous solubility is the major problem encountered with formulation development of new chemical entities (NCEs) and is becoming increasingly challenging.² Amorphous active pharmaceutical ingredients (APIs) are often advantageous compared to the corresponding crystalline forms due to better solubility, faster dissolution, and the resulting better oral bioavailability. Ever since the 1960s, amorphous solid dispersions (ASD), which consist of amorphous APIs dispersed in a polymeric crystallization inhibitor, have been utilized as a formulation strategy that enhances the bioavailability of poorly water-soluble drugs by increasing their dissolution rate.^{3,4} It enables a possibly high drug loading below the critical supersaturation in the polymer matrix, which significantly restricts drug mobility.⁵ Molecular level mixing can be achieved by multiple methods including spray drying (SD) and hot melt extrusion (HME).^{6,7} However, a major problem with ASDs is the risk of eventual conversion of the amorphous form to a more stable crystalline form, either through direct crystallization from supersaturation, or after amorphous-amorphous phase separation. Microscopic properties including molecular mixing and homogeneity have significant impacts on physicochemical stability as well as dissolution profiles.8-12 Molecular dispersion of drug substances in the polymer matrix has been proposed to minimize recrystallization by decreasing the molecular mobility. 13-15 Intermolecular API-polymer interactions in ASDs have been shown to play a critical role in the formation of a drug-rich phase as a colloidal dispersion in solution, which impacts the dissolution process. 16,17 Therefore, it is crucial to understand the molecular mixing of APIs with polymers in ASDs and mechanisms of ASD stabilization and destabilization, for instance related to humidity. 18,19

There are a number of thermodynamic, optical and vibrational spectroscopic as well as microscopic techniques for probing phase separation in pharmaceutical systems. $^{20-26}$ Detection of a single glass-transition temperature (T_g) in differential scanning calorimetry (DSC) has been considered as the "gold standard" for establishing miscibility or at least mixing. However, DSC is not able to detect phase separation on length scales smaller than 30 nm. 27 A single T_g from DSC may be misleading and not sufficient to indicate a homogeneous mixture. 10,28,29 For example, while a single glass transition has been identified for itraconazole and hydroxypropyl methylcellulose (HPMC) ASDs at up to 50% drug loadings, suggesting good miscibility, 21 atomic force microscopy (AFM) coupled with nanoscale infrared spectroscopy and nanothermal analysis (AFM-nanoIR-nanoTA) has successfully identified phase separation in these systems on the submicron scale. 30,31 Optical and vibrational imaging can provide high chemical contrast, but the spatial resolution is typically diffraction-limited to >100 nm and the penetration depth, e.g. of IR and Raman analyses, is often <1 μ m. 30 Fluorescence microscopy has also been successfully utilized for the

characterization of miscibility but requires the addition of fluorophores for differentiating chemical components.^{21,28,32} Moreover, high-resolution imaging techniques, such as scanning electron microscopy and AFM, are restricted to the particle surface, cannot determine concentrations, and often require specific sample preparation.

In addition, a mixed system is not necessarily homogeneous. Molecularly mixed domains with different local drug loadings can coexist.^{30,31} Compared to the characterization of molecular mixing, it is of significant technical challenge to identify and quantify heterogeneity. Li et al. have successfully utilized atomic force microscopy-based nanoscale thermal analysis (nanoTA) to investigate local compositions, e.g. size and location of drug-rich phases, of lopinavir/HPMC ASDs.³¹ Interestingly, their results suggest that the identified heterogeneities can improve the in-vitro release of lopinavir at a drug loading >33%. Therefore, these microstructures related to both molecular mixing and homogeneity play critical roles in impacting the physical stability as well as the drug release mechanisms. High spatial resolution (<100 nm) and quantitative characterization techniques are needed to provide this valuable information. In particular, an analytical method to quantify inhomogeneity and composition of bulk and "as-is" ASD samples at a high resolution is of great interest.

Solid-state nuclear magnetic resonance (ssNMR), using nuclear spins as local structural probes, can provide both chemical resolution and domain-size information, and has been successfully applied in evaluation of polymer mixtures $^{33-35}$ and of mixing in ASDs. 28,29,36,37 . These pharmaceutical applications evaluate the API–polymer mixing by comparing 1 H spin-lattice relaxation times (T_{1H} as well as $T_{1\rho H}$) of the two components and providing an estimated domain size based on simplistic assumptions such as uniform mixing or complete phase separation. For example, the 1 H spin-lattice relaxation method has been utilized to assess the indomethacin and HPMC mixing and successfully correlated it with the mechanical energy input of the HME processes. 29 Compared to the 1 H relaxation method, 1 H spin diffusion NMR 33,38,39 can more quantitatively determine intermolecular distances and has been utilized in polymers $^{40-42}$ and biological systems 43 .

In this study, we have, for the first time, adapted the spin-diffusion NMR method to quantify both mixing and inhomogeneity of ASDs. Our results demonstrate that ASD domain sizes on the nanometer scale and phase compositions can be quantified from the time dependence of polymer signal recovery due to ¹H spin diffusion from the API. The model system studied consists of nifedipine (Nif), an antihypertensive drug that binds to a calcium channel, and polyvinylpyrrolidone (PVP), a commonly used polymeric excipient. Nif/PVP ASDs have been extensively utilized as model systems of molecular mixing

in previous publications including thermal dynamic analysis^{8,23} and NMR relaxation studies.^{36,44-46} To probe the distribution of the ¹H magnetization with good functional-group resolution, ¹³C detection after cross polarization (CP) from ¹H is used. Incomplete mixing, e.g. due to large polymer-rich domains of at least a few tens of nanometers in diameter, is manifested in terms of incomplete equilibration of the magnetization after long spin diffusion times; in other words, the initially suppressed signals do not reach the same relative intensity as in the unselective spectrum. This effect is enhanced and thus made more convincing by partial inversion of magnetization in one of the components. We reveal homogeneous mixing in a sample with low drug-loading (DL) made by SD, and probe inhomogeneous mixing in all high DL samples made from either SD or HME in terms of incomplete equilibration and differential ¹H spin-lattice relaxation (*T*_{1H}). Moreover, AFM is applied to confirm the presence of domains deduced from ssNMR. A model of two mixed phases of different compositions is developed to quantitatively explain the experimental results and confirm the consistency of incomplete equilibration and differential relaxation, shedding light on the mixing in ASDs on the sub-100-nm level.

2. Materials and Methods

Materials and Preparation of ASDs

Nifedipine (Nif), 13 C-labeled Nif (1,4-dihydro-2,6-dimethyl-4-(2-nitrophenyl)-3,5-pyridine-2,3,5,6- 13 C₄-dicarboxylic- 13 C₂ acid dimethyl ester), and polyvinylpyrrolidone (PVP, molecular weight = 360 kg/mol, MDL number MFCD00149016) were purchased from Sigma-Aldrich (St. Louis, MO). Two sets of Nif-PVP ASDs were prepared by spray drying (DL = 5%, 20%, 40% and 60%) and by hot melt extrusion (DL = 40%), as described below.

Preparation of HME samples started with generating binary physical mixtures (PM) of Nif-PVP with a weight ratio of 40:60 (DL = 40%) by blending in a Turbula mixer at 100 rpm. In a typical procedure, ~200 g of the mixture was sealed in a 500 mL glass bottle and mixed for 60 min at room temperature (25 °C). The extrusion was performed on a customized benchtop twin screw extruder (MP&R™ Model ME7.5) with co-rotating 7.5 mm conveying screws (L/D=15). In a typical process, ~40 g of a physical mixture of Nif-PVP was fed into the extruder by using a vibratory feeder. The barrel temperature was set to 186 °C, and the screw speed to 100 rpm. The hot melt extrudates were collected, allowed to cool in air, and milled into powder.

Spray-dried ASDs at 5% DL were prepared on a ProCepT 4M8-TriX spray dryer equipped with a 0.8 mm two-fluid nozzle (ProcepT, Zelzate, Belgium). Briefly, Nif and PVP were co-dissolved in methanol at a total solid concentration of approximately 18 mg/mL. The solution was then sprayed at a rate of 5.0

mL/min and atomized using compressed air at 70 psi. Inlet and outlet air temperatures were set to be 100 and 50 °C, respectively. The drying air was maintained at a flow rate of 0.1 m³/min. ¹³C labeled and unlabeled Nif were mixed at a 1:4 weight ratio for preparing the 5% DL sample (¹³C-Nif/PVP SD). PVP was pre-dried overnight in a vacuum oven. The produced ASD was not post-dried.

Atomic Force Microscopy

Cross-sections of milled hot-melt extrudate particles composed of 40% by weight nifedipine in PVP (186 °C) were prepared for AFM analysis by mounting a single particle in a micro-vise and sectioning with an EM UC7 ultramicrotome (Leica) and a glass knife. The flat faced particles were imaged with a Cypher ES atomic force microscope (Asylum Research) within an environment of 10% or less relative humidity maintained by an RH-200 (L&C Science and Technology). AFM imaging was performed in alternating contact (tapping) mode with ArrowUHFAuD cantilevers (Nano World) driven at resonance photothermally via BlueDrive while maintaining net repulsive sample–tip interactions. Scan rates were typically 5 to 6 Hz and images were collected at 512×512 pixel resolution. First order X-Y plane fits were applied to images as necessary to correct for sample tilt. Data analysis was performed in DragonFly Pro 4.1. The images were loaded with a custom loader able to import 512×512 pixel AFM data. The pixel size was set to 1.95 nm. For image segmentation, the DragonFly implementation of the k-means algorithm⁴⁷ as implemented from Scikit⁴⁸ was used to classify the data into three classes based on the unbiased algorithm. This algorithm achieved an effective separation of the dark domains into a distinct class. Subsequently, a connected components analysis was performed on the dark regions to separate single domains. Finally, the mean Feret diameter for each domain was computed.

Solid-state NMR

The ¹H and ¹³C NMR experiments were conducted at resonance frequencies of 400 MHz and 100 MHz, respectively, using a Bruker DSX400 spectrometer and a 4-mm magic angle spinning (MAS) probe head. The ¹³C chemical shift was referenced to TMS, using the carboxyl group in glycine at 176.49 ppm as a secondary reference. The ¹H chemical shift was referenced to the hydroxyl proton resonance of hydroxyapatite at 0.18 ppm. NMR experiments were carried out to obtain 1D ¹H and ¹³C spectra, ¹H spin diffusion with ¹³C detection and corresponding build-up curves, and ¹³C-detected ¹H *T*₁ relaxation data, as described in the following.

Direct polarization ¹H NMR spectra without probe-head background signal were collected with a simple pulse-length-doubling probe-head background suppression scheme published previously.⁴⁹ After

one-pulse excitation, a 2-ms 1 H spin-lock can be used as a rotating-frame spin-lattice-relaxation (T_{1pH}) filter to selectively suppress the magnetization of bound water associated with PVP. 13 C-detected 1 H inversion-recovery was conducted by inserting a variable 1 H T_{1} relaxing period after a 1 H inversion pulse, followed by ~ 1 -ms cross polarization (CP) 50,51 to transfer the relaxed 1 H magnetization to 13 C. With a recycle delay of 10 s, it took ~ 40 h to collect a full series of 1 H inversion-recovery spectra with excellent signal-to-noise ratios, and ~ 20 h (6,400 scans) more for a spectrum near the zero crossing. An experiment with a double, 1 H 2-ms T_{1p} and ~ 20 -µs T_{2H} , filter followed by spin diffusion and CP to 13 C is described in the following section. Each doubly filtered spectrum typically took ~ 4 h (3,072 scans) to record, but longer for the sample with the lowest (5%) Nif fraction ($\sim 24,000$ scans). The 90° pulse lengths for 1 H and 13 C were 3.7 µs and 4 µs, respectively. Frequency-switched Lee-Goldburg (FSLG) homonuclear decoupled 1 H- 13 C HETCOR⁵² experiments with 0.01 ms, 10 ms, or 300 ms 1 H spin diffusion periods and 0.5-ms CP were conducted on 5 wt% Nif/PVP SD and 40 wt% Nif/PVP 186 °C HME samples. 10 h and 24 h of signal averaging was sufficient to collect HETCOR spectra with 0.01 ms and 300 ms spin diffusion, respectively, with good signal-to-noise ratios. All experiments were performed at ambient temperature at a MAS frequency of 7 kHz, except for 1 H- 13 C HETCOR at 7.5 kHz.

3. Results and Discussion

The major goal of this study was to investigate molecular mixing and inhomogeneity of spray-dried and hot-melt extruded NIF/PVP ASDs by means of a convenient high-resolution spin-diffusion NMR method. We start by establishing theoretical correlations between spin diffusion time traces and scenarios of phase separation. One-dimensional (1D) and two-dimensional (2D) ¹H spin diffusion NMR experiments are then designed to probe the distribution of Nif and PVP in a quantitative manner. These spin diffusion results are compared and combined with the widely utilized NMR spin-lattice relaxation measurements using a numerical model for quantifying the drug loadings of large mixed domains of two different compositions.

3.1 Preliminary ASD Characterizations

As preliminary characterization of Nif-PVP ASDs, we have utilized scanning electron microscopy (SEM) to examine the morphology, and powder X-ray diffraction (PXRD) as well as DSC to detect the crystallinity. Experimental details are summarized in supporting information. SEM analysis of the spraydried amorphous materials in **Figure S1** confirmed particle morphologies composed of hollow and deformed spheres, as expected and common for this manufacturing method. Representative diffraction patterns and a thermal diagram of the nifedipine-PVP ASD extruded at 186 °C are shown in **Figures S2**

and S3, respectively. The data demonstrate that this extrudate lacks crystallinity and has a single T_g at 100.4 °C, much reduced from the value near 180 °C in neat PVP.

3.2 Mixing and Inhomogeneity Probed by Spin Diffusion NMR

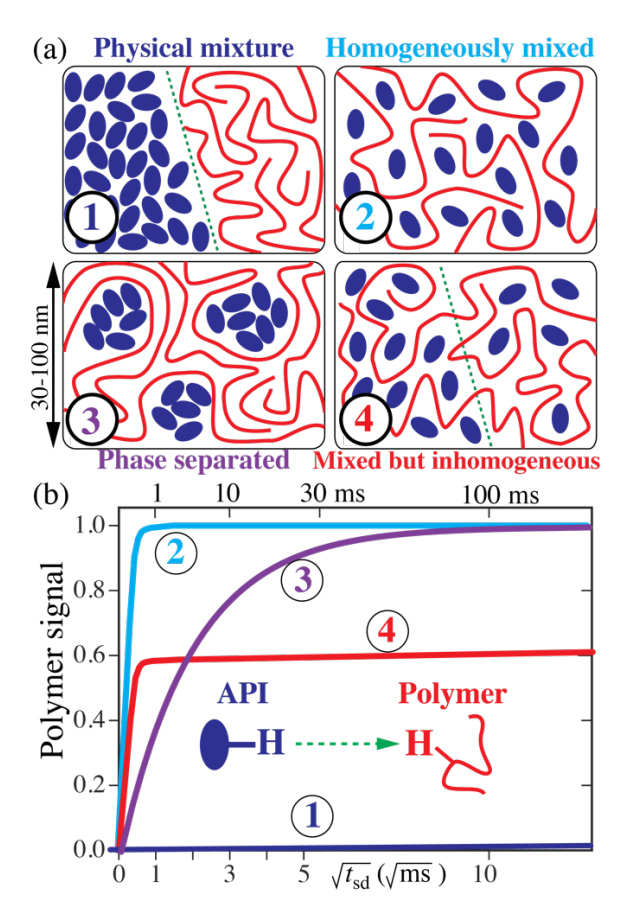


Figure 1. Different models of mixing of API and polymer excipient molecules (blue ellipses and red lines, respectively) and corresponding NMR responses due to ¹H spin diffusion from the API. (a) Four different mixing models are shown: (1) a physical mixture, (2) a homogeneously mixed system, (3) phase separation forming small domains, and (4) two large molecularly mixed phases of different compositions. (b) Recovery of polymer signal by ¹H spin diffusion after initial selective suppression for the four cases shown in (a).

In this study, we applied several ssNMR techniques utilizing 1 H spin diffusion to probe the mixing of nifedipine and PVP on the molecular to nanometer scale. In rigid amorphous organic solids whose $T_{\rm g}$ is much higher than room temperature, including PVP and its ASD with Nif, most chain mobility is "frozen in" and there is no large-amplitude motion of chain segments that would time-average the 1 H- 1 H dipolar

couplings. These strong couplings result in fast spin exchange among the protons in ASDs, which can be described as a diffusive process⁵³ with a spin diffusion coefficient of $D \le 0.8$ nm²/ms.^{33,54} Once ¹H spin polarization of a certain component within a sample, for example PVP in this study, is suppressed through a suitably designed radio-frequency (rf) pulse sequence, ¹H spin diffusion from nearby Nif molecules will bring the ¹H polarization distribution back towards the uniform equilibrium distribution. The more finely dispersed Nif and PVP are, the more quickly the polarization of the suppressed component recovers, which is most conveniently observed in a ¹³C spectrum after cross polarization from ¹H to ¹³C. Thus one can estimate the domain sizes of the components up to a few dozen nanometers from the time constant of the observed PVP signal recovery.^{33,54} In addition, whether the suppressed component reaches equilibrium, i.e. whether the spectrum after a long spin diffusion time matches the unselective ¹³C spectrum, gives valuable information about the homogeneity of the system.

To facilitate our later discussion and better explain our approaches, we analyze four relatively simple models of API and excipient mixing, as illustrated in **Figure 1**. Suppose one prepares an ASD composed of one single type of API molecules (illustrated as blue ellipses) and a polymeric excipient (illustrated as red lines). Depending on the relative affinity of API and polymer and the procedure for making the ASD, the dispersion of the API molecules in the polymer can be very different. An extreme case would be a physical mixture of the two components, with grains of API on the micron to millimeter scale imbedded in the polymer, which corresponds to case 1 in **Figure 1a**. After polymer ¹H magnetization is suppressed, spin diffusion from the API can reach as far as 20-60 nm across the API–polymer interface; nevertheless, the majority of API and polymer molecules in this model are out of reach and no noticeable polymer signal recovery would be detected by NMR (case 1 in **Figure 1b**). Another extreme case would be API and polymer mixed homogeneously at the molecular level throughout the whole sample. In such a system, case 2 in **Figure 1**, a fast recovery of polymer signal would be observed, and the intensity should be in equilibrium with the API within 1 ms of spin diffusion, since the average distance between API and polymer molecules is only a few Å.

It is not particularly remarkable that ssNMR can distinguish a physical mixture from a homogeneously mixed system, since many other techniques can achieve this, including DSC with a resolution down to the ~30 nm level. However, ssNMR has a unique capability to establish contrast between phases at the nanometer scale and identify a molecularly mixed but inhomogeneous system. At the onset of amorphous phase separation, the formation of small pure API particles embedded in the polymer matrix would be difficult for DSC to identify, whereas spin diffusion would easily pick them up through the slow signal recovery of the polymer, due to the increased distance from the interior of the API particles to

polymer matrix (case 3 in **Figure 1**). At last, we want to propose the mixed but inhomogeneous system, which would be a natural result of a miscibility gap from thermodynamics. At least two domains, one API-rich and the other API-poor, coexist in such a system, and each is a molecularly mixed and homogeneous phase (case 4 in **Figure 1**). Such a model can be viewed as consisting of two mixed and homogeneous domains with different local drug loadings, where polymer molecules in each domain are reached by spin diffusion from their own API partners and would exhibit a fast initial signal recovery. However, since the polymer in the API-poor domain hardly gets supplied with ¹H polarization from the API molecules in the API-rich domain, the total polymer signal never reaches equilibrium with API, resulting in a "scaled down" recovery curve of the homogenously mixed system, as shown by the red curve (case 4) in **Figure 1b**. In order to make spin diffusion detectable, NMR techniques are needed that selectively suppress polymer magnetization and monitor the reappearance of the polymer signal; this is described in the following.

3.3 One-Dimensional Double-Filter Spin Diffusion NMR

The pulse sequence developed for detecting ¹H spin diffusion between Nif and PVP is shown in Figure 2a. It features a ¹H double filter followed by ¹H spin diffusion and cross polarization to ¹³C for highresolution detection. After a ¹H 90° excitation pulse, a 2-ms T_{10H} filter is inserted before a 20- μ s or 25- μ s dipolar-evolution (T_{2H}) filter. During a subsequent spin diffusion time, the remaining ¹H magnetization on Nif is allowed to diffuse as far as ~30 nm. Finally, the ¹H magnetization is transferred to ¹³C by CP for better spectral resolution. As a starting point, a steep gradient of ¹H magnetization is generated, where PVP is fully suppressed, while Nif magnetization remains. This is achieved by selective suppression of the ¹H magnetization of PVP by 20- μ s ¹H T_{2H} filtering. The structures of Nif and PVP in **Figure 2a** show that methylene (-CH₂-) groups are abundant in PVP but absent from Nif. The strong ¹H dipolar coupling in immobilized methylene results in shorter T_{2H} in PVP than in Nif. It is worth noting that such a gradient of ¹H magnetization through T_{2H} filtering is quite commonly achievable in ASDs, since APIs are often rich in aromatic CH and in methyl (-CH₃) groups, while polymeric excipients are typically abundant in methylenes. Figure S4 confirms that the PVP signals were removed from the spectrum of a 40 wt% Nif/PVP physical mixture after a 20- μ s T_{2H} filter, and did not reappear after 100-ms spin diffusion, as predicted in case 1 in Figure 1. This indicates that the 20-µs dipolar-evolution filter selectively suppressed PVP magnetization as intended. Series of spectra from 40 and 60 wt% Nif/PVP SD after a 20-µs T_{2H} filter (but no T_{10H} filter) as a function of spin diffusion time, see Figure S5, showed spin diffusion to PVP reaching equilibrium in 30 ms, but little if any magnetization loss of Nif. This suggests an invisible source of 'H magnetization, which was indeed identified in ¹H NMR spectra.

¹H NMR spectra of 40 wt% and 60 wt% Nif/PVP SD with 2-ms $T_{1\rho H}$ filtering (**Figure S5b,d**) reveal a second component with a smaller line width than Nif that needs to be considered. The small line width corresponds to a long T_{2H} , which means that this magnetization will survive the T_{2H} filter. The intensity of this peak near 4 ppm was variable in intensity between different samples (**Figure S6**), being generally correlated with the PVP fraction and lower in the HME than in the SD sample with 40% Nif loading. Based on these observations, the mobile component, which was invisible in direct-polarization ¹³C spectra, was identified as H₂O. Short $T_{1\rho H}$ indicates motional rates near 10⁶/s, as characteristic of bound water. This signal was thus assigned to bound H₂O associated with PVP. Based on its short $T_{1\rho H}$ relaxation time shown in **Figure S6**, it can be suppressed quite easily by a 2-ms spin lock ($T_{1\rho H}$ filter) preceding the T_{2H} filter. Relaxation of PVP and Nif during the spin lock occurs with a much longer $T_{1\rho H}$ relaxation time of ~20 ms.

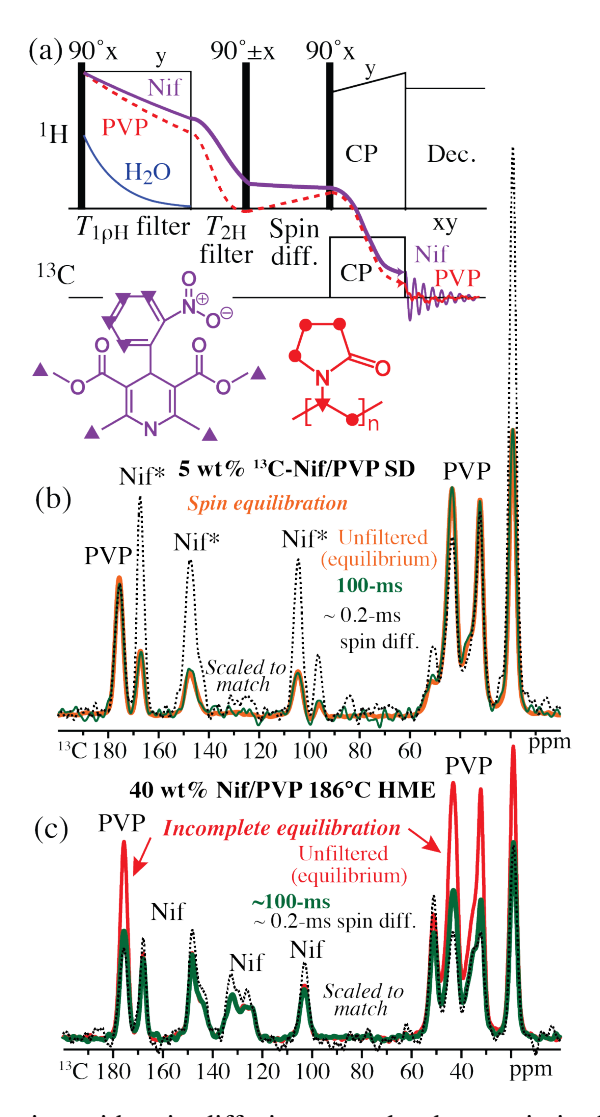


Figure 2. (a) ¹H double filtering with spin diffusion to probe the proximity between Nif and PVP. The

double-filter pulse sequence suppresses 1 H magnetization of bound water (blue curve) by a T_{1pH} filter and of PVP (red dashed curve) by a T_{2H} filter. The remaining Nif magnetization (purple curve) diffuses to nearby PVP, whose signals reappear accordingly. The structures of Nif and PVP are also shown, with CH₂ groups (short T_{2H}) marked by circles and CH or CH₃ moieties (longer T_{2H}) by triangles. The successful suppression of the PVP signal in a physical mixture by a 20- μ s T_{2H} filter is shown in Figure S4. (b, c): Unfiltered spectra (solid orange or red lines), and spectra after the 1 H double filter with minimal ~0.2 ms (dashed black lines) and with 100 ms (solid green lines) spin diffusion are compared for (b) 5 wt% Nif/PVP SD (with peaks enhanced by 13 C-labeling marked by asterisks), and (c) 40 wt% Nif/PVP 186 $^{\circ}$ C HME. The unfiltered spectra (solid orange or red lines) are scaled to match the aromatic Nif peaks in the spectra after 100-ms spin diffusion.

After the 2-ms $T_{1\rho \rm H}$ and 20- μ s $T_{2\rm H}$ double filtering, ¹H magnetization is allowed to diffuse from Nif to adjacent molecules. One can roughly estimate the average distance r between the magnetization source (Nif) and the sink (PVP) from the spin diffusion time $t_{\rm sd}$ needed to reach local equilibrium, assuming $r = \sqrt{6Dt}$ and a ¹H spin diffusion coefficient of $D \le 0.8$ nm²/ms in a rigid proton-rich solid^{33,54}. The data for 5 wt% Nif/PVP SD provide a good example of homogeneous mixing of Nif and PVP. ¹H double filtering suppressed PVP magnetization, and spin diffusion from Nif during the 1 ms CP (~ 0.2 ms of effective spin diffusion)^{33,54} partially recovered PVP, shown in the black dashed spectrum (**Figure 2b**). ¹H magnetization from Nif then locally equilibrated all nearby PVP within 3 ms of spin diffusion corresponding to average domain sizes of less than $\sqrt{6 \square 0.8}$ nm²/ms $\square 3$ ms $\square 4$ nm.

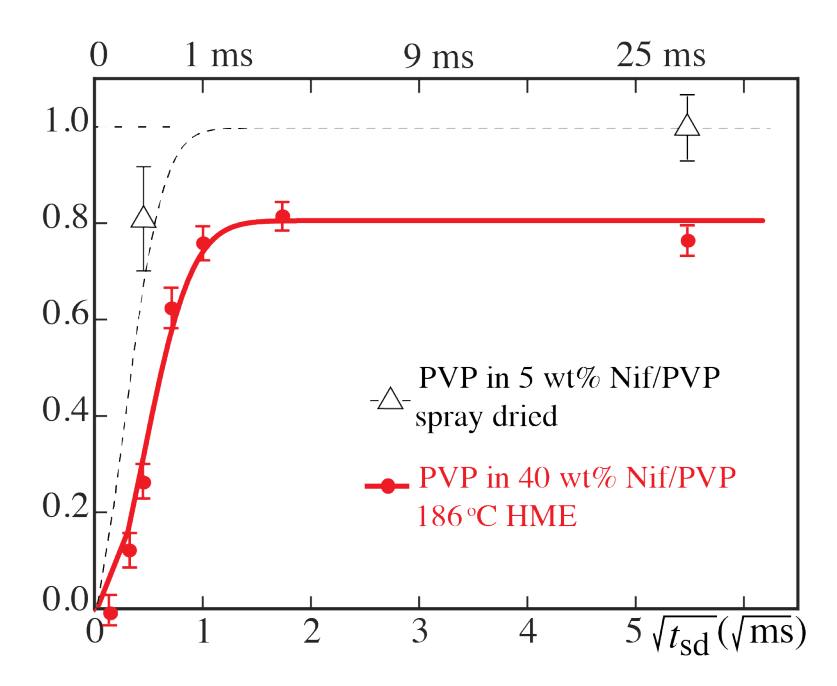


Figure 3. Recovery of PVP signal through spin diffusion after a double filter in 40 wt% Nif/PVP HME (filled red circles and solid red line) and in 5 wt% Nif/PVP SD (open triangles and dashed black line).

The behavior observed in 40 wt% Nif/PVP HME was distinctly different. While spin diffusion redistributed some ¹H magnetization from Nif to PVP, with Nif decreasing while PVP increased, indicating some mixing, it did not reach global equilibrium as highlighted in Figure 2c. The discrepancy from equilibrium suggests that at least two domains with different Nif contents exist with diameters of at least a few tens of nanometers. When the PVP signal intensity is normalized based on total spectral integration and plotted as a function of the spin diffusion time, Figure 3, it becomes obvious that this corresponds to case 4 in Figure 1, where the ASD is molecularly mixed but inhomogeneous. Similar incomplete equilibration is observed in all the other ASDs except for 5 wt% Nif/PVP SD (see Figure S7). One should note that the proton density in Nif is lower than in PVP, and the average ¹H distance between Nif and PVP at the contact interface is larger than within PVP. As a result, the actual spin diffusion coefficient D should be smaller than 0.8 nm²/ms. In other words, our distance estimate should be taken as an upper bound, accurate within a factor of two. The normalized recovery curve of the PVP signal in Figure S8, compared with the recovery of the thiomethylene signal in U-13C-L-methionine (~0.3 nm domain size) and crystalline methylene in single-crystal polyethylene (PE) (~2 nm amorphous-layer thickness), makes it clear that spin diffusion from Nif to PVP is fast, comparable to that in methionine. This indicates molecular-level but inhomogeneous mixing of Nif and PVP. Similar fast but incomplete equilibration is observed in other Nif/PVP samples as well, as shown in **Figures S7 and S8**.

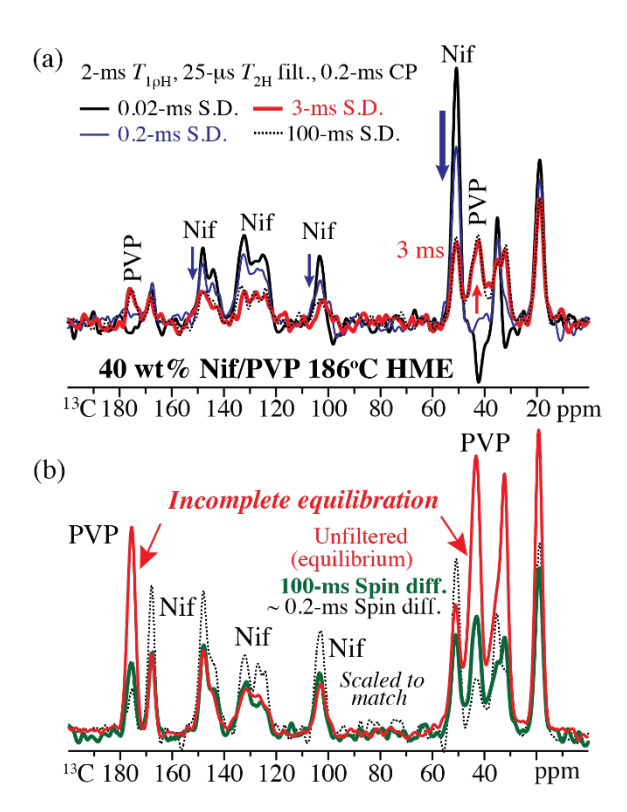


Figure 4. Incomplete equilibration of 40 wt% Nif/PVP 186 °C HME made more obvious by an inverting 25-μs T_{2H} filter after 2-ms $T_{1\rho}$ filtering. (a) Inverting filter made visible in short-CP 13 C spectra collected with various spin diffusion times. (b) Pronouncedly incomplete equilibration after the inverting filter, 100 ms of spin diffusion, and regular 1-ms CP.

The incomplete equilibration of magnetization by spin diffusion from Nif to PVP was rather unexpected. The effect can be amplified, and thus corroborated, by partial inversion of the PVP 1 H magnetization. As mentioned earlier, after 20 μ s of dipolar evolution, the 1 H magnetization of PVP crosses zero, whereas after 25 μ s, it is inverted. While the inverted signal in a dipolar evolution is only a few percent of the total, the PVP inversion effect is amplified by the concomitant partial dipolar dephasing of the Nif magnetization. For instance, if the Nif magnetization after 25 μ s is +20% and the PVP magnetization -5%, after rescaling the Nif magnetization to 100% the PVP inversion is -25% and thus substantial. The inversion can only be observed after short CP, since otherwise spin diffusion during 1-ms CP obscures the inversion effect. After 0.2-ms CP, the partial inversion of PVP by a 25- μ s T_{2H} filter is clearly seen in the spectra of **Figure 4a**. It quickly recovers while Nif decreases as the spin diffusion time is increased to 3 ms, and remains unchanged until 100 ms. The inversion reduces the PVP signal in a manner that persists after spin diffusion and thus amplifies the deviation from global equilibrium in the spectra with long CP after a long spin diffusion time, see **Figure 4b**.

3.4 Two-dimensional Spin Diffusion NMR

ASDs by measuring the API–polymer proximity.⁵⁵ Nanometer-scale mixing can also be probed by 2D 1 H- 13 C HETCOR NMR with 1 H spin diffusion. In this experiment, the 1 H polarization encoded with 1 H chemical shift information is spread out to nearby protons through spin diffusion, and then transferred through cross polarization to nearby 13 C for detection. Whereas the double filter relies on the difference of relaxation properties between Nif and PVP, in 1 H- 13 C HETCOR NMR the contrast is based on sufficiently large 1 H chemical shift differences, for instance between the aromatic protons in Nif and the alkyl protons in PVP. While this experiment is more demanding to set up and generally takes more spectrometer time than the double-filter experiment, it is still a valuable alternative when T_{2H} contrast is insufficient, and it is broadly applicable as APIs commonly contain aromatic protons resonating at >7 ppm, while the methylene protons abundant in polymeric excipients resonate below 3 ppm. As expected, in **Figure S9a** and **b** both 1D slices taken at 2.6 ppm from 5 wt% Nif/PVP SD and 40 wt% Nif/PVP 186 $^{\circ}$ C HME 2D HETCOR were characteristic PVP 13 C spectra, while a projection around the 1 H aromatic chemical shift showed mainly Nif signals, with minor PVP signals resulting from $^{\circ}$ 0.1-ms spin diffusion during the 0.5 ms CP time.

In 5 wt% Nif/PVP SD, 300 ms of spin diffusion equilibrated the ¹H magnetization in the HETCOR NMR spectrum (see **Figure 5a**), as ¹H magnetization from all sources polarized ¹³C in Nif and PVP equally well. This confirms the homogeneous mixing deduced from ¹H double filtering and spin diffusion in this sample. On the other hand, the HETCOR spectrum in **Figure 5b** shows that in 40 wt% Nif/PVP 186 °C HME the ¹H spins of Nif did not polarize ¹³C in PVP as well as PVP ¹H did, and vice versa, confirming the inhomogeneous mixing revealed previously by the ¹H double-filter experiment. Nevertheless, comparison of the 2D HETCOR spectra without and with spin diffusion (**Figure S9**) clearly demonstrates some ¹H spin diffusion between Nif and PVP and thus corroborates our earlier results.

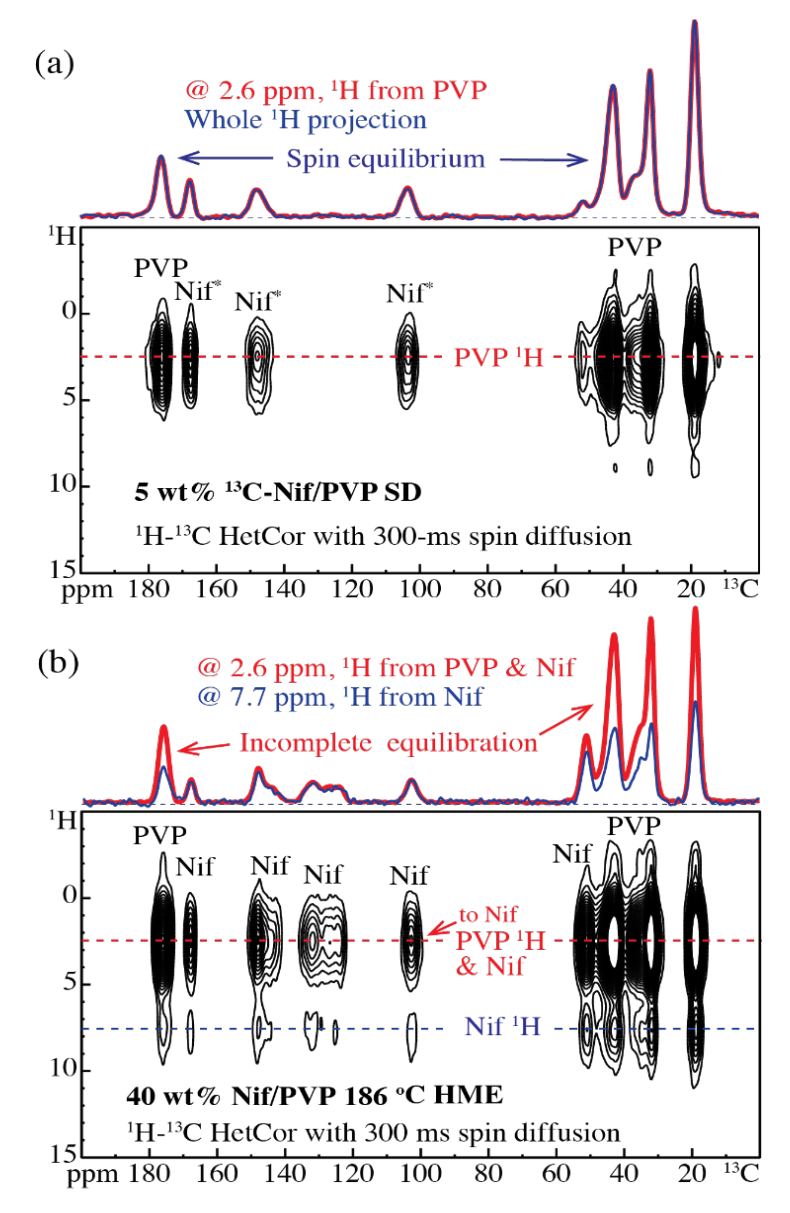


Figure 5. ¹H-¹³C HETCOR spectra after 300-ms spin diffusion of (a) 5 wt% Nif/PVP SD and (b) 40 wt% Nif/PVP 186 °C HME. Above each 2D spectrum, cross sections at the alkyl 2.6 ppm proton resonance are shown in blue (thin line) and compared with the overall spectrum in part a) and with the cross section at the aromatic-proton resonance (7.7 ppm) in part b) (thick red lines).

3.5 Differential ¹H Spin-Lattice Relaxation

 1 H double filtering or 1 H- 13 C HETCOR with spin diffusion are methods useful for probing and quantifying phase separation. However, these experiments may not always be applicable for routinely monitoring mixing in established pharmaceutical systems, because they require sufficient contrast in T_{2H} values or in 1 H chemical shifts. The ssNMR relaxometry method offers an alternative by measuring a 1 H

longitudinal relaxation time using 13 C 28,29,36,37 or 1 H detection 35 . Briefly, the 1 H spin-lattice relaxation time in the laboratory frame (T_{1H}) or rotating frame (T_{1p}) can be utilized to probe phase separation with domain sizes of roughly 20-100 nm and 1-20 nm, respectively, based on representative values of $T_{1H} = 1$ s and $T_{1p} = 10$ ms for amorphous APIs and a spin diffusion coefficient of $D = 8.0 \times 10^{-12}$ cm²/s = 0.8 nm²/ms. For instance, in the system studied here the intrinsic T_{1H} value of PVP (≤ 2 s) is significantly different from that of Nif (≥ 4 s). If the 1 H relaxation times of API and polymer components in an ASD are more similar than those of the pure components, this is evidence of some mixing.^{28,36}

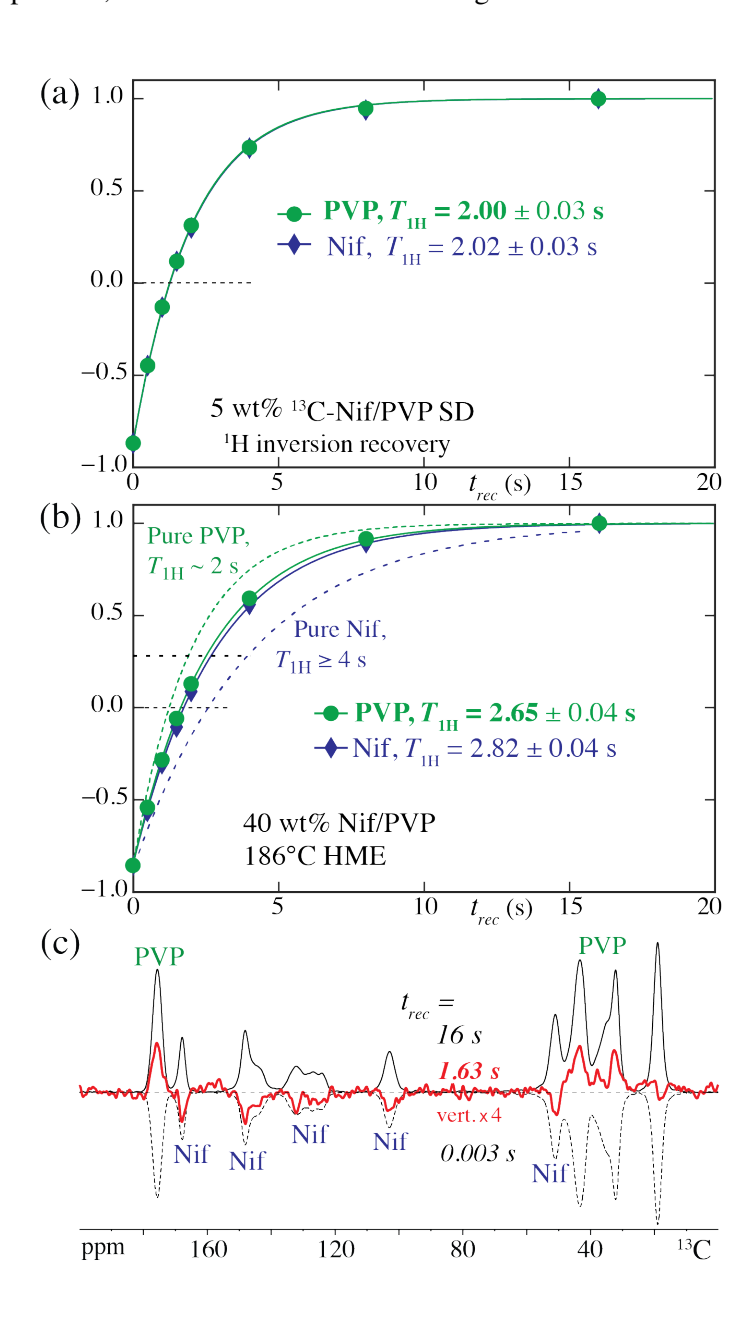


Figure 6. ¹³C-detected ¹H inversion recovery, where (a) indistinguishable ¹H inversion recovery of Nif (blue diamonds) and PVP (green dots) in 5 wt% Nif/PVP SD, and (b) differential T_{1H} relaxation in 40 wt% Nif/PVP 186 °C HME. (c) The differences in the T_{1H} relaxation times are highlighted near the zero crossing after 1.63 s of recovery (red line), four-fold vertically expanded compared to the initial magnetization (dashed line) and the equilibrium spectrum (solid black line).

While $T_{\rm 1H}$ measurements have been previously used to characterize phase separation in ASDs, 28,36 we expand their utility to systems with small differences in the observed relaxation times of the two components. Going beyond simplistic formulas that take the root-mean-square displacement of the magnetization within the relaxation time as a stand-in for a domain size or choose an arbitrary relaxation time cut-off for miscible vs. immiscible systems, below we present a quantitative analysis that provides more structural detail.

¹H saturation or inversion recovery can be used to probe T_{1H} relaxation. We have chosen inversion recovery after a ¹H 180° pulse and a recovery delay, before a read-out pulse and cross polarization to ¹³C for easy detection with high chemical-shift resolution. As expected, the homogenously mixed 5 wt% Nif/PVP SD produces indistinguishable Nif and PVP ¹H recovery curves and T_{1H} values, shown in **Figure 6a**. Nif and PVP in 40 wt% Nif/PVP 186 °C HME have slightly different T_{1H} values (**Figure 6b**). Near the zero-crossing recovery time, the reality of the small relaxation-time differences can be shown convincingly: **Figure 6c** shows a spectrum (in red) in which the Nif signals remain inverted while the PVP signals have already become positive.

3.6 Domain Imaging by AFM

A representative AFM alternating contact (tapping mode) phase image of a milled hot melt extrudate particle composed of 40% nifedipine in PVP is shown in **Figure 7a**. The particle was freshly sectioned with an ultramicrotome prior to imaging to yield an ultra-smooth surface with average roughness of approximately 1 nm over the 1 µm × 1 µm scan area of the image. Contrast in the phase image is the result of the AFM tip interacting with local regions of differing mechanical properties due primarily to compositional differences of the material at this length scale and is consistent with phase separation of the drug–polymer mixture. Image analysis was performed to extract the Feret diameters of the distributed domains (dark regions in the image), and their distribution is shown in **Figure 7b**. This can be converted into the corresponding distribution of the area fraction as a function of domain size, **Figure 7c**, which is more relevant for comparison with NMR, since a domain of twice the diameter and four times the area contributes four times more strongly to the NMR signal.

It is important to note that the AFM image represents a 2-dimensional cross-section of the material and determining their true 3-dimensional size and shape distribution requires a variety of assumptions and application of stereological analysis. For example, a 2D cross section of monomodal spheres randomly distributed in a 3D matrix yields a distribution of circles whose average radius underestimates the true radius, which would actually be the largest value measured in that case. For polydisperse spheres and non-spherical shapes, generating 3D models from 2D cross sections is yet more complicated and out of scope for this study. Nevertheless, the AFM image shown here clearly shows phase separation with domain sizes and center-to-center distances on the order of 20 nm, consistent with the NMR data.

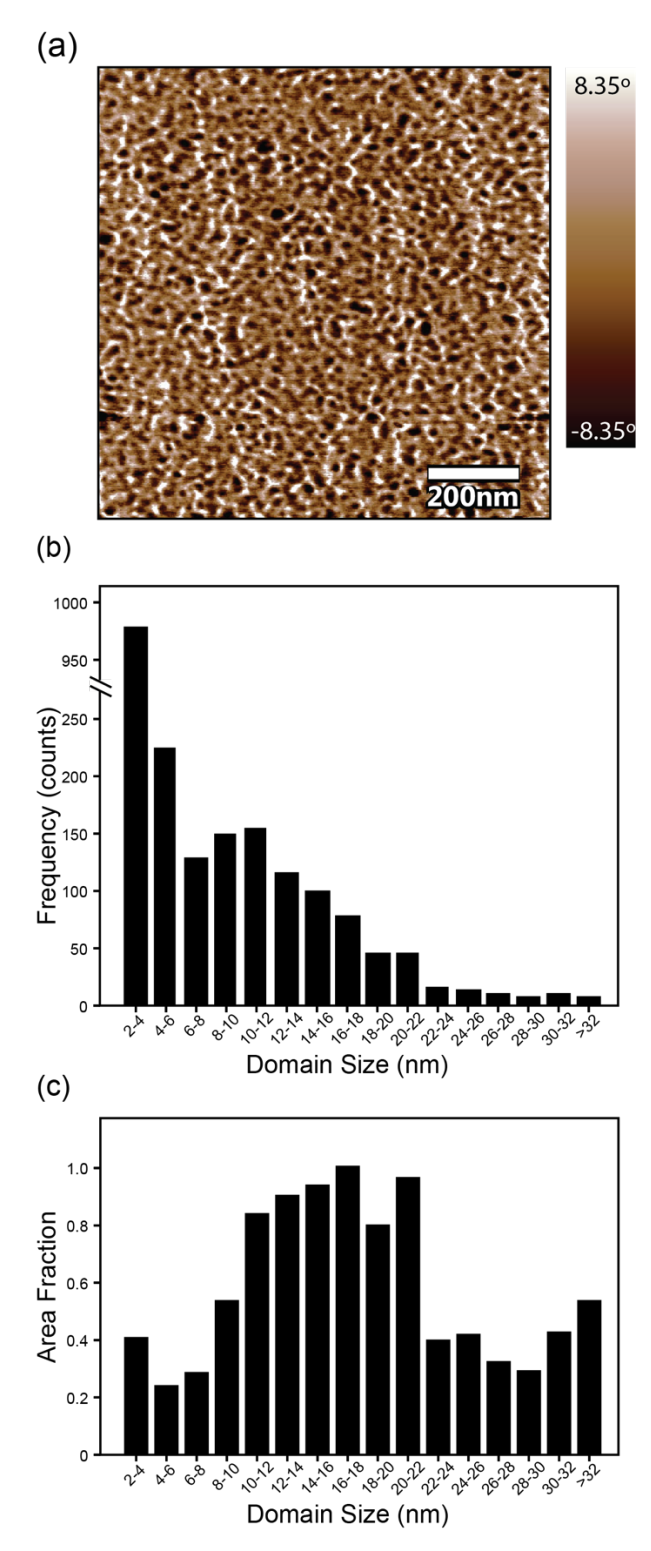


Figure 7: (a) AFM phase image of 40% nifedipine in PVP hot melt extrudate (186 °C) particle cross-section. (b) Distribution of Feret diameters of the distributed domains (dark areas) within the AFM phase image. (c) Area fraction (frequency multiplied by square of domain size and normalized) as a function of domain size.

3.7 Quantitative NMR Analysis of Nif/PVP Inhomogeneity

Most previous studies have utilized relaxation measurements for probing phase separation and semi-quantitatively estimating the domain size. One critical goal of this study is to quantify the phase composition, besides the identification of molecular mixing or phase separation. While the fast transfer of magnetization between Nif and PVP shows their mixing on the molecular scale, the lack of global equilibration by 'H spin diffusion documents incomplete mixing, or inhomogeneity, on a scale a few tens of nanometers. A number of different structural models are consistent with the observations and are included in the following quantitative analysis. Thermodynamics of mixing would predict a miscibility gap between a Nif-poor and a Nif-rich phase. The Nif-poor and therefore PVP-rich mixed phase should contain a substantial amount of Nif, due to stabilization by entropy of mixing, while the Nif-rich phase should be nearly pure Nif, since the positional entropy of the polymeric PVP is small. The domains of these phases must be larger than the spin-diffusion range (~20 nm). In this model, polarization does not globally equilibrate since the magnetization from the Nif-rich phase does not reach PVP in the PVP-rich phase.

3.7.1 Model of two mixed domains

An intuitively appealing model amenable to quantitative analysis posits two types of large domains or phases made up of intimately mixed PVP and Nif, in different proportions (see **Figure S10a**). Simply put, in this model the return of the PVP signal is incomplete since the PVP-rich domains, which contain little Nif, are barely polarized by spin diffusion from Nif. This is seen most easily in terms of the missing PVP intensity if the Nif peaks are scaled to match as in **Figures 2c** and **4b**.

We characterize the morphology in terms of the Nif weight fractions $w_{\text{Nif,1}}$ and $w_{\text{Nif,2}}$ in the two domains and the weight fractions μ_1 and $\mu_2 = 1 - \mu_1$ of the two domains in the sample. The overall weight fraction of Nif, w_{Nif} , is known, e.g. 0.4, and it is complementary to the overall PVP weight fraction, $w_{\text{PVP}} = 1 - w_{\text{Nif}}$. These quantities are related by a linear weighted-averaging relation:

$$w_{\text{Nif}} = \mu_1 \ w_{\text{Nif},1} + \mu_2 \ w_{\text{Nif},2} = \mu_1 \ w_{\text{Nif},1} + (1 - \mu_1) \ w_{\text{Nif},2}$$
 (1)

see also eq.(S6). **Figure 8** shows the relevant parameter space in terms of the composition of the Nif-rich region, $w_{\text{Nif,2}} \ge w_{\text{Nif}}$, along the horizontal axis and of the Nif-poor region $w_{\text{Nif,1}} \le w_{\text{Nif}}$ along the vertical direction. This implies $w_{\text{Nif,1}} \le w_{\text{Nif,2}}$: If one phase is Nif-depleted (relative to the average w_{Nif}), the other must be Nif-enriched. The rectangle shown in **Figure 8** is the region of the full space $(0 \le w_{\text{Nif,1}} \le 1, 0 \le w_{\text{Nif,2}} \le 1)$, see the small overview at the top of **Figure 8**) that is consistent with the overall composition. The upper left corner $(w_{\text{Nif,}}, w_{\text{Nif}})$ in **Figure 8** is on the diagonal of the full space and corresponds to a uniform

sample of the average composition w_{Nif} since both domains have the same composition. Points near it correspond to large-scale composition fluctuations of moderate amplitude, for instance as found at intermediate times in spinodal decomposition. The space of nearly uniform composition also extends out from the corner along the adjacent sides of the rectangle. The lower right corner (100%, 0) corresponds to complete phase separation into pure-Nif and pure-PVP domains. Above it is the region corresponding to a typical miscibility gap. The right edge corresponds to pure Nif coexisting with a mixed phase, the bottom edge to a pure PVP phase coexisting with a mixed phase. A core–shell structure produced by diffusion of Nif into large PVP particles would correspond to regions near the bottom of the rectangle.

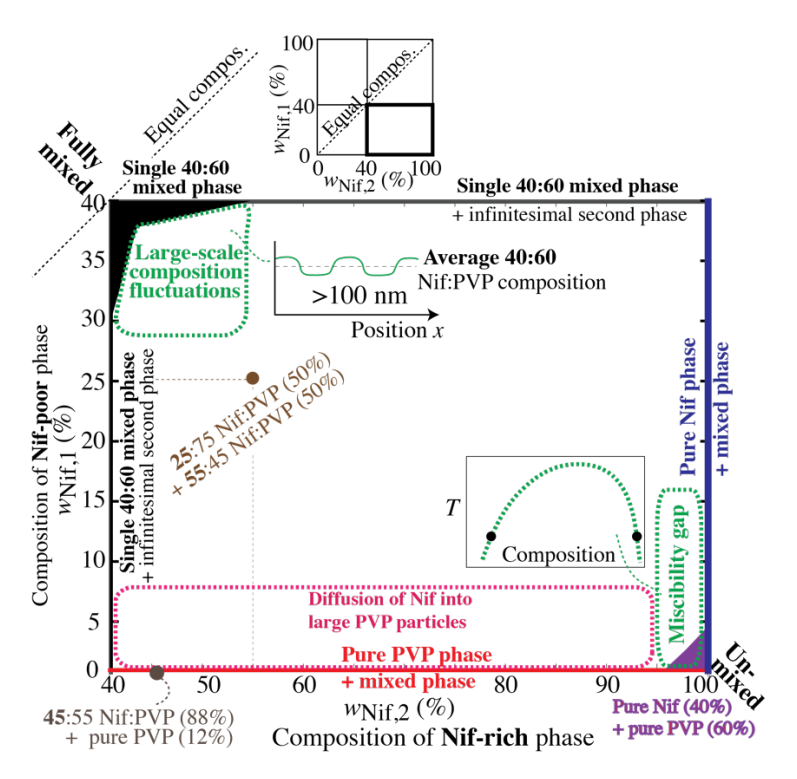


Figure 8. The possible compositions in a two-mixed-phases model with $w_{\text{Nif}} = 0.4$ expressed in composition parameter space. Several regions corresponding to specific formation processes are highlighted near the corners and edges of the diagram, while a pair of example compositions are specified (in brown). The coloring used at the edges and corners is for contrast and clarity.

We treat $w_{\text{Nif},1}$ and $w_{\text{Nif},2}$ as the independent variables and solve eq.(1) for the domain weight fraction μ_1 in terms of these variables and the given parameter w_{Nif} :

$$\mu_{1} = (w_{\text{Nif}} - w_{\text{Nif},2})/(w_{\text{Nif},1} - w_{\text{Nif},2}) \tag{2}$$

The plot of the weight fraction of the PVP-rich domain 1 across the composition space according to eq.(2), with straight contour lines converging in the upper left corner, is shown in **Figure S10b**.

In the following, asymptotic spin diffusion levels and T_{1H} relaxation times of Nif and PVP are calculated for all points in the interior of the rectangle, i.e. all different possible pairs of mixed domains, and the experimentally observed values are marked in the diagrams; compositions compatible with the experimental asymptotic spin diffusion levels and T_{1H} relaxation times can thus be read off the diagrams. Since the relaxation analysis will be more familiar to most readers, it is presented first.

3.7.2 T_{1H} relaxation in two mixed domains

Since Nif is mixed with PVP on a molecular scale, ${}^{1}H$ spin diffusion during the course of typically seconds of ${}^{1}H$ longitudinal relaxation (T_{1H}) is long enough to average the intrinsic relaxation rates $1/T_{1,PVP}$ and $1/T_{1,Nif}$ within a given domain or phase. The $T_{1,n}$ in phase n (for n = 1, 2) can thus be calculated from the weighted average of the relaxation rates,

$$1/T_{1,n} = H_{PVP,n}/T_{1,PVP} + H_{Nif,n}/T_{1,Nif} \qquad (n = 1, 2)$$
(3)

where $H_{\text{Nif,n}}$ is the proton fraction of Nif in phase n. It is fairly close to the corresponding Nif weight fraction $w_{\text{Nif,n}}$ and can be calculated from it as described in the SI (eqs.(S16) and (S17)). To evaluate eq.(3), we assume that $T_{1,\text{PVP}}$ is similar as in neat PVP (1.8 to 2.4 s); how this value is constrained and that its uncertainty is quite insignificant is discussed below and demonstrated in the SI (eqs.(S19) and (S20)). Then the unknown $T_{1,\text{Nif}}$ of amorphous Nif can be estimated from the measured effective $T_{1\text{H}}$ of the sample overall by solving the rate-averaging equation

$$1/T_{1H} = H_{PVP}/T_{1,PVP} + H_{Nif}/T_{1,Nif}$$
(4)

for $T_{1,\text{Nif}}$, where H_{Nif} is the proton fraction of Nif in the sample overall. Given that at a slightly lower field strength than ours, amorphous Nif has a T_{1H} of 4.2 s and amorphous Nif in 95:5 and 90:10 Nif:PVP has an observed ^{1}H spin lattice relaxation time of 4.4 s, 36 the amorphous $T_{1,\text{Nif}}$ value in our experiments is expected to be between 4 and 6 s. It is useful to note that equation (4) provides a completely general constraint on the shorter intrinsic relaxation time:

$$1/T_{1H} > H_{PVP}/T_{1,PVP} \quad \Rightarrow \quad T_{1,PVP} > H_{PVP} T_{1H} \tag{5}$$

For instance, for 40 wt% Nif/PVP 186 °C HME we have $H_{PVP} = 0.7$ and observed $T_{1H} = 2.73$ s, so eq.(5) requires $T_{1,PVP} > 1.91$ s. Additional useful constraints on the intrinsic relaxation times are discussed in the SI (eqs.(S19) and (S20)).

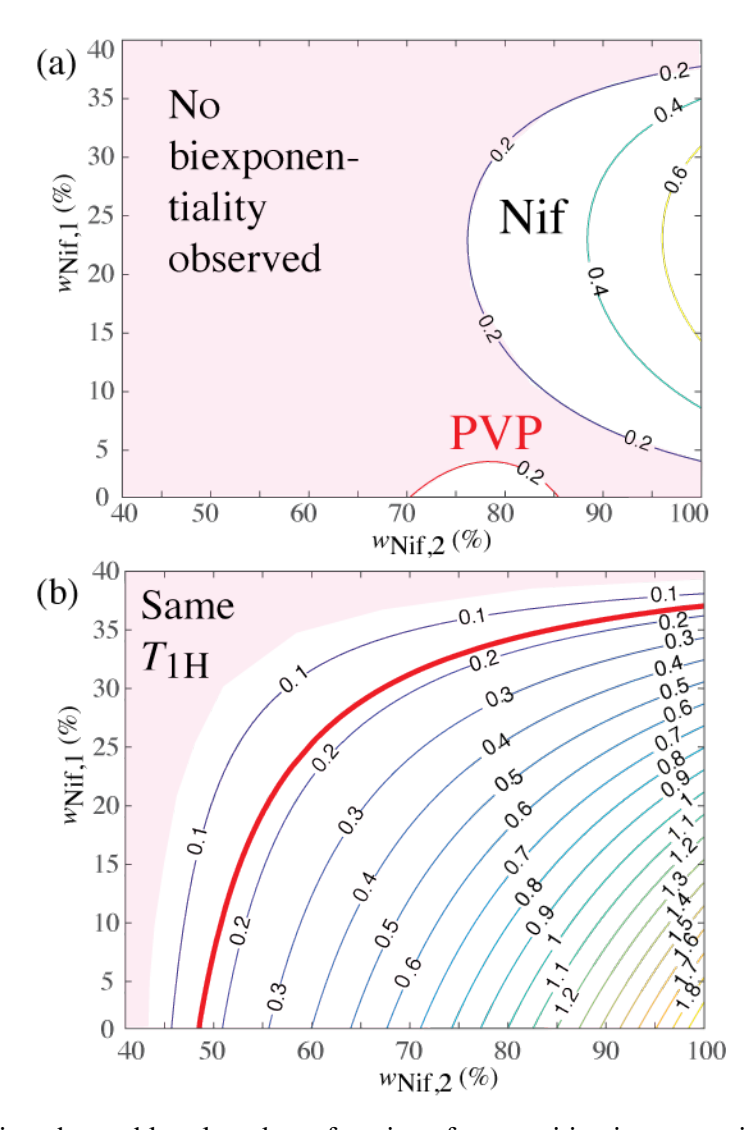


Figure 9. $T_{\rm 1H}$ relaxation observables plotted as a function of composition in a two-mixed-phases model, for $w_{\rm Nif} = 0.4$ and $T_{\rm 1Nif} = 4.4$ s. (a) Biexponentialities (quantified as percent root-mean-square deviations from the best exponential fit) of PVP and Nif ¹H inversion recovery calculated using eq.(6) in a combined plot. No significant biexponentiality was observed experimentally. (b) Difference $\Delta T_{\rm 1H}$ between $T_{\rm 1H}$ of Nif and PVP, ranging between 0 and 3 seconds, calculated for ¹H inversion recovery experiments using eq.(7) and preceding equations, contour plotted in the reduced composition parameter space. The experimentally observed $\Delta T_{\rm 1H}$ value of 0.17 s (see Figure 6c) is highlighted by a thick red line. The individual plots of $T_{\rm 1H}$ of Nif and of PVP are shown in Figure S11.

The relaxation curve of Nif during inversion recovery is given by the weighted superposition of the relaxation of Nif in phase 1 and phase 2:

$$S_{\text{Nif}}(t) = [h_1 H_{\text{Nif},1} (1 - 2 \exp(-t/T_{1,1})) + h_2 H_{\text{Nif},2} (1 - 2 \exp(-t/T_{1,2}))]/H_{\text{Nif}}$$
(6a)

with the proton fractions of the two phases, h_1 and h_2 (defined in eq.(S8c) and expressed in terms of the Nif weight fractions via eqs.(S12), (S16), and (S18a)), which are analogous to the domain weight fractions μ_I in eq.(1) (see also **Figure S10a**). For PVP,

$$S_{PVP}(t) = [h_1 H_{PVP,1} (1 - 2 \exp(-t/T_{1,1})) + h_2 H_{PVP,2} (1 - 2 \exp(-t/T_{1,2}))]/H_{PVP}$$
(6b)

Accordingly, the relaxation of each component is biexponential. However, the deviations from single-exponential relaxation are often small. The fits to the experimental data shown in **Figure 6b**, which exhibit no detectable biexponentiality, were generated according to eq.(6), with domains of 25/75 and 56/44 Nif/PVP composition and 50:50 weight fractions, compatible with $w_{\text{Nif}} = 0.4$. The relaxation curves with maximum biexponentialities for Nif and PVP with $w_{\text{Nif}} = 0.4$, $T_{1,\text{PVP}} = 2.2$ s and $T_{1,\text{Nif}} = 5.5$ s are shown in **Figure S11**. **Figure 9a** shows contour plots of the biexponentialities as a function of the Nif weight fractions in the two phases. The maximum biexponentiality of Nif relaxation occurs where a pure Nif phase ($w_{\text{Nif},2} = 1$) with its long $T_{1\text{H}}$ coexists with a roughly equal amount of a mixed phase that contains significant PVP shortening $T_{1\text{H}}$ and enough Nif to produce a strong enough Nif signal contribution. Because the biexponentiality is generally small, it is possible to define effective spin lattice relaxation times by

$$S_{PVP}(T_{1eff,PVP}) = (1-2/e), S_{Nif}(T_{1eff,Nif}) = (1-2/e).$$
 (7)

Figure S12a shows a contour plot of $T_{\text{leff,Nif}}$, obtained by evaluating eqs.(S16), (3), (S12), (S16), (S18a), (6), and (7) with $T_{\text{lNif}} = 5.5 \text{ s}$, and $T_{\text{lPVP}} = 2.2 \text{ s}$ systematically as a function of $w_{\text{Nif,1}}$ and $w_{\text{Nif,2}}$ for a given overall composition $w_{\text{Nif}} = 0.4$. The values range from 5.5 s for phase separated amorphous Nif to 2.73 s in a uniform mixture. The corresponding plot for PVP is shown in **Figure S12b**. The range of $T_{\text{leff,Nif}}$ values consistent with experiment, see **Figure 6b**, centered on 2.82 s, for 40 wt% Nif/PVP 186 °C HME is highlighted. The most robust relaxation quantity³⁶ is the difference

$$\Delta T_{1H} = T_{1\text{eff,Nif}} - T_{1\text{eff,PVP}} \tag{8}$$

between the Nif and PVP relaxation times. The plot of $\Delta T_{\rm 1H}$ in the composition space (the difference of $T_{\rm 1eff,Nif}$ and $T_{\rm 1eff,PVP}$ values as plotted in **Figures S12a** and **S12b**) is shown in **Figure 9b**. It is quite insensitive to the exact values of the intrinsic relaxation times used in the analysis. **Figure S13** documents that for $\Delta T_{\rm 1H}$ < 0.5 s (dark blue curves), all possible absolute values of $T_{\rm 1,PVP}$ and $T_{\rm 1,Nif}$ produce fairly similar arcs of $\Delta T_{\rm 1H}$ in the composition space.

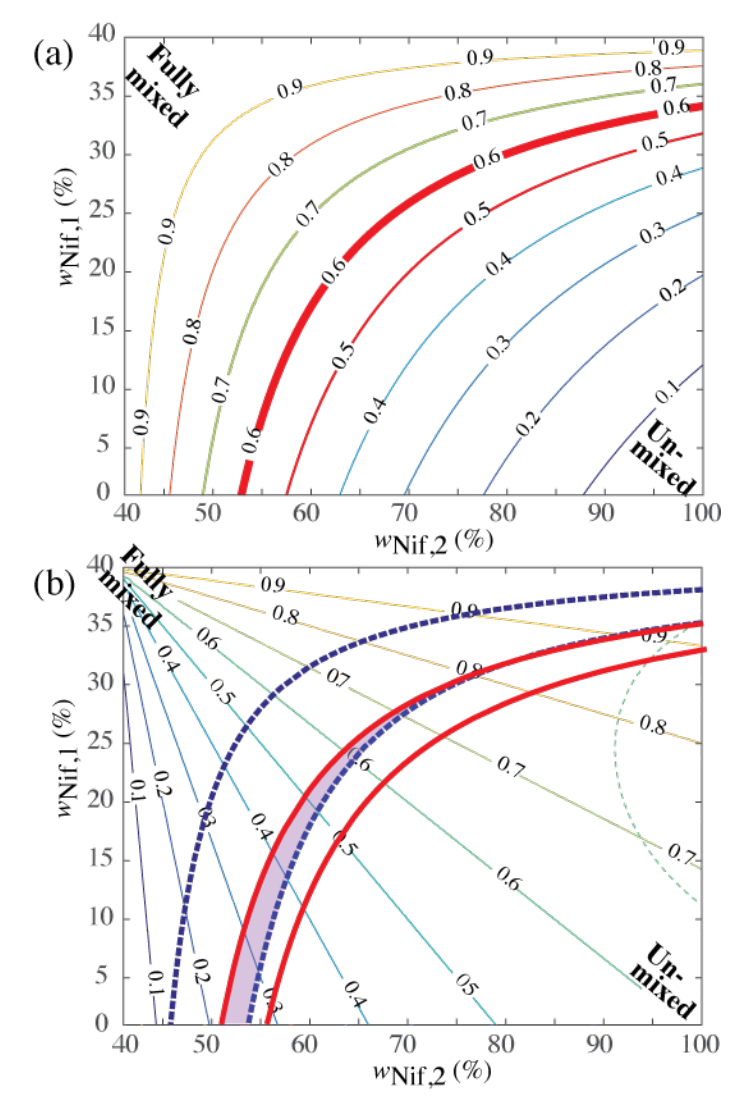


Figure 10. NMR observables plotted as a function of compositions in a two-mixed-phases model, for w_{Nif} = 0.4, calculated using eqs.(9-11) and (3). (a) Mixing parameter that can be deduced from long-time intensity ratios in spin diffusion experiments as defined in the text. The value of MP = 0.6 observed after double filtering in Figure 2c, and confirmed by HETCOR NMR, of 40 wt% Nif/PVP 186 °C HME is highlighted as a thick red line. (b) Constraints from relaxation ($\Delta T_{\text{1H}} = 0.17 \pm 0.07$ s, see Figure 6c; dashed blue outline) and spin diffusion ($MP = 0.6 \pm 0.05$, thick red outline) combined give the shaded area representing possible compositions, superimposed on a contour plot of the weight fraction of the PVP-rich

domain 1. T_{INif} = 4.4 s was assumed in the relaxation analysis. To the right of the thin green dashed curve is a region with more biexponentiality than experimentally observed.

3.7.3 Spin-diffusion "equilibration" in two mixed domains

The final intensities of "exchange" PVP peaks E_{PVP} and of Nif source or "diagonal" signals D_{Nif} after initial PVP (and H_2O) ¹H suppression and spin diffusion, as shown in **Figures 2b,c** and **4b**, can be predicted in the two-mixed-domains model. The analysis may be easiest to understand by referring to the corresponding conceptual 2D exchange diagrams in **Figure S14**. In phase n, the Nif diagonal intensities after local equilibration are $H_{Nif,n}$ ². Weighted with the proton fractions of the domains, these account for the intensity of the overall Nif source or "diagonal" signal after local equilibration:

$$D_{\text{Nif,long}} = h_1 H_{\text{Nif,1}}^2 + h_2 H_{\text{Nif,2}}^2 \tag{9}$$

The quantities on the right-hand side can be calculated using eqs.(S12) and (S16). The exchange-peak intensity in phase n is $H_{\text{Nif,n}}$ $H_{\text{PVP,n}}$ and therefore the overall PVP signal after a long spin diffusion time is

$$E_{\text{PVP,long}} = h_1 H_{\text{Nif,1}} H_{\text{PVP,1}} + h_2 H_{\text{Nif,2}} H_{\text{PVP,2}}$$
(10)

These final intensities in eqs. (9) and (10) can be used to calculate a mixing parameter MP according to

$$MP = E_{\text{PVP,long}}/D_{\text{Nif,long}} \left(H_{\text{Nif}}/H_{\text{PVP}} \right) \tag{11}$$

which is unity for a single uniform phase, and zero for coexisting pure-Nif and pure-PVP domains. MP is the ratio of the PVP peaks in the overlayed spectra with Nif peaks matched by scaling as shown in **Figure 2c** (see the SI, eqs.(S21)-(S24), for the proof). **Figure 10a** shows a contour plot of the mixing parameter MP calculated using eqs.(S12), (S16), and (9-11) as a function of composition in terms of $w_{\text{Nif,1}}$ and $w_{\text{Nif,2}}$. The range of MP consistent with experiment for 40 wt% Nif/PVP 186 °C HME is highlighted by thick red outlines in **Figure 10b** and superimposed with the relaxation results (dashed blue outlines).

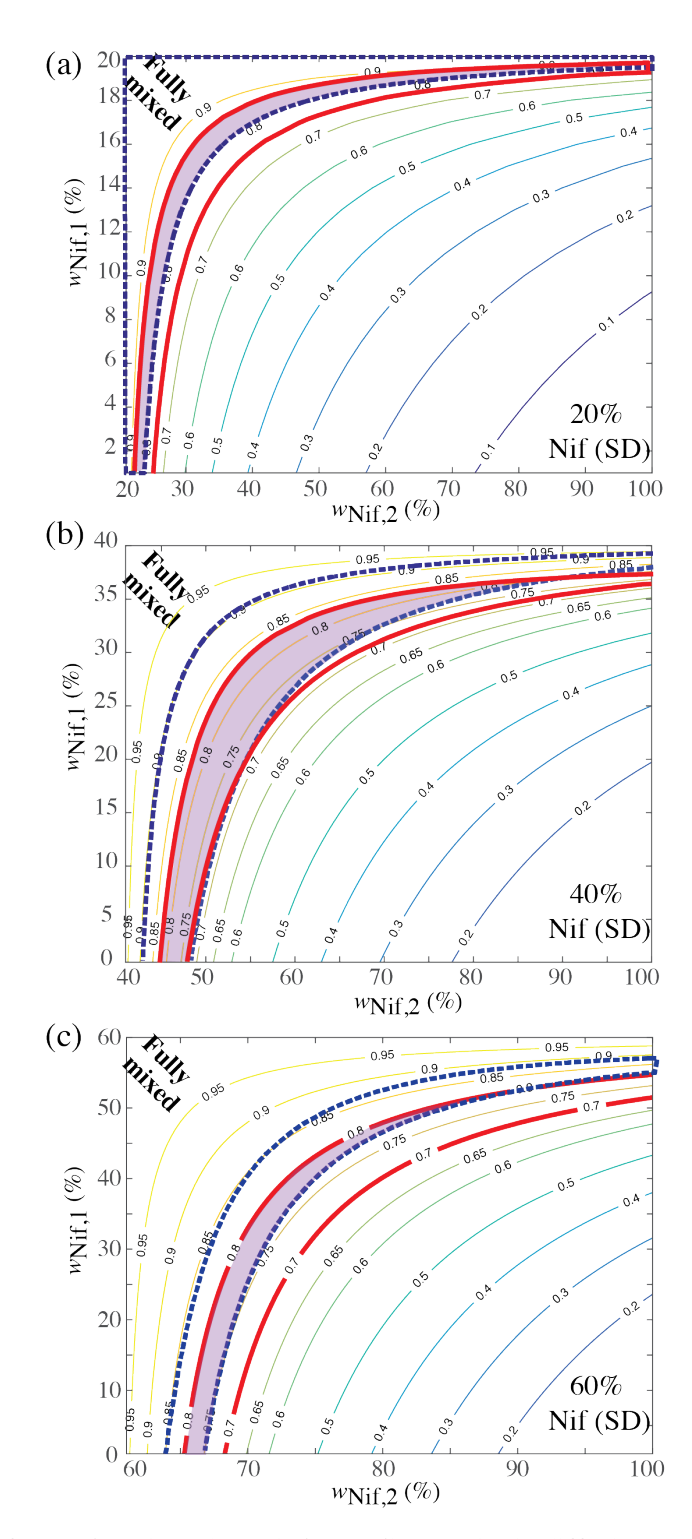


Figure 11. Constraints from relaxation (dashed blue outline) and spin diffusion (thick red outline) combined give the shaded area representing possible compositions in a two-mixed-phases model, for spray-dried Nif/PVP with weight fractions of (a) 20:80, (b) 40:60, and (c) 60:40. $T_{1Nif} = 4.4$ s was assumed in the relaxation analysis.

3.7.4 NMR analysis of spray-dried samples

The results of the combined NMR analysis for three spray-dried Nif/PVP ASD samples are shown in **Figure 11**. The mixing parameter is 0.80 ± 0.05 for the sample with 20% Nif, while the materials with 40% and 60% Nif have $MP = 0.75 \pm 0.05$, see **Figure S7**. The agreement between spin diffusion after double filtering and relaxation analysis assuming $T_{1\text{Nif}} = 4.4 \text{ s}$ is seen to be good in **Figure 11**. The mixing parameters here are significantly higher than in the HME sample, indicating that spray drying produced less inhomogeneous materials than hot-melt extrusion.

It is worthwhile to compare our findings with a previous miscibility study of similar Nif–PVP ASD systems.³⁶ Yuan et al. measured 1 H relaxation times in a series of ASDs with high Nif concentrations in PVP. A certain level of relaxation time difference was chosen as an artificial dividing line between miscible and immiscible ASDs. The 95:5 and 90:10 Nif:PVP samples were declared to be immiscible, even though the observed near-doubling of T_{1H} of PVP must be attributed to the influence of nearby slowly-relaxing Nif, proving mixing on the <20-nm scale. We have pointed out here that a system can be molecularly mixed yet inhomogeneous, with two mixed phases as the simplest case.

3.7.5 Synopsis of NMR analyses

The incomplete global equilibration seen in spin diffusion experiments and differential $T_{\rm IH}$ revealed by $^{\rm I}$ H inversion recovery both show that high-Nif-fraction Nif/PVP ASDs are inhomogeneously mixed. The combination of all the NMR constraints in **Figure 10b** and **11** are consistent, for instance, with 40 wt% containing 15 wt% Nif coexisting with 60 wt% containing 56 wt% Nif, or with a nearly pure PVP phase of ~20% mass fraction coexisting with a ~50:50 mixed phase that accounts for 80% of the mass. The inhomogeneity is more pronounced in the hot-melt-extruded than in the corresponding spray-dried sample. AFM imaging confirms ~20-nm phase separation in 40 wt% Nif/PVP 186 $^{\circ}$ C HME, as shown in **Figure 7**.

3.8 Relaxation and Spin Diffusion NMR Applications in Pharmaceutical Science

Molecular miscibility has often been proposed to impact physical stability and dissolution profile of APIs and therefore utilized to facilitate the design of formulation processes. PXRD and DSC are two routine tools that have been widely used to evaluate the mixing of polymer–API ASDs.²³ Specifically, the absence of sharp peaks in powder X-ray diffraction (PXRD) patterns and the appearance of a single T_g in the DSC thermogram are generally considered as the criteria of forming ASDs. However, due to fundamental limitations of the diffractometer and calorimeter, simply relying on these two techniques is not sufficient to reliably discriminate a homogeneously mixed polymer-API system from molecularly mixed but heterogeneous samples. The representative PXRD and DSC data in **Figure S2** and **S3** show no

crystalline diffraction peaks and melting peaks, respectively, of the API when the extrusion temperature is at 186 °C, which agrees well with the broad peaks in 13 C NMR spectra (**Figure 2**). In the reversible heat flow curves of DSC, which is a routine tool for evaluating the apparent miscibility in ASDs, only a single T_g is detected. Within the experimental limitations of the calorimeter and using a conventional interpretation, this would suggest a fully miscible system. However, as ssNMR and AFM have shown, in most of the samples studied here, Nif and PVP were not homogeneously mixed on the 20-nm scale.

API recrystallization represents a major risk to the physical stability of ASDs. It is well recognized that $T_{\rm g}$ cannot be utilized as a reliable indicator to predict stability.⁵⁶ The amorphous-to-crystalline conversion of APIs in a glassy state (i.e. below T_g) has often been observed. Moreover, phase separation is known to be a major driving force of the destabilization of ASDs in supersaturated glasses or liquids.¹⁰ The prediction of long-term stability is often a challenge due to the lack of a high resolution tool that can identify key attributes like molecular mixing. Despite of efforts to utilize modeling and theoretical calculation to understand and predict miscibility and stability, 9,59,60 the community is constantly seeking for experimental parameters for such purpose. The ssNMR relaxation method was originally developed to evaluate mixing of polymers in the 1990s, 33,40 introduced to pharmaceutical applications in the 2000s, 61,62 and widely utilized for the semi-quantitively characterization of ASDs in the past decade. 28,29,36,37,63,64. For example, Ma et al. prepared a few ASDs of nifedipine and poly(vinylpyrrolidone-co-vinyl acetate) (PVP/VA64) via HME at different specific mechanical energy (SME) inputs. 45 These extrudates exhibited an identical single T_g value of 89 °C but can be differentiated by T_{1H} and T_{1pH} . The relaxation results suggest that ASDs produced at a relatively lower SME are not mixed and becomes partially mixed at a higher energy input. Higher energy input of the HME process has been demonstrated to improve the mixing of indomethacin (IND) and HPMC, which correlates well with the enhanced dissolution process.²⁹ In a study by Purohit et al., a correlation was established between the mixing of itraconazole (ITZ) and hydroxypropyl methylcellulose (HPMC) ASDs and the kinetics of solvent evaporation.²⁸ These previous examples have evaluated mixing and estimated the size of phase-separated domains in a semi-quantitative manner. Our current study has further advanced the relaxation method and developed 1D and 2D spin-diffusion NMR techniques to quantitatively measure the domain size as well as the phase composition, for evaluating both mixing and inhomogeneity.

The nature of the inhomogeneity, e.g. two mixed phases of different compositions, quantified in our study was not properly recognized by relaxation measurements in previous ssNMR studies. A conventional model with most Nif in nearly pure domains of ~10-nm diameter (lower right edge in **Figure 10b**), where spin diffusion would equalize T_{IH} values but cannot do so on the much shorter ${}^{1}H$ T_{1p} time scale, is excluded by our data. Accordingly, Nif and PVP in the 40 wt% Nif/PVP 186 °C HME sample

exhibit essentially the same T_{1pH} relaxation time. The data in **Figure 10b** are consistent (at the left bottom edge) with ~20 wt% of more or less pure PVP coexisting with a ~50:50 Nif:PVP molecular-level mixture whose spin-lattice relaxation would be dominated by the higher relaxation rate of PVP.

It is also worth noting that ¹H NMR shows that there is absorbed water in the ASD produced by HME at elevated temperature (186 °C) (**Figure S6**). Whereas the ¹H spin-lattice relaxation method is affected by H₂O-driven spin relaxation, the T_{1pH} filter utilized in our spin-diffusion experiment can effectively remove the impact of water on the analysis of mixing by NMR. This is particularly useful when measuring stability samples stressed under high humidity.

The quantitative measurement of bulk ASD samples at sub-100 nm resolution can be utilized to identify phase separation at an early stage, make a selection on the kinds and grades of carrier polymers, and investigate how physiochemical parameters, e.g. humidity and temperature, and formulation processes impact physical stability. The high-resolution quantification of small domains may also offer an opportunity to further explore the fundamental mechanism of nucleation and crystal growth of drugs in supersaturated solid solution.⁶⁵

4. Conclusions

In this study, we developed a 1 H-double-filtering ssNMR experiment with 1 H spin diffusion and 13 C detection to study the mixing of nifedipine and PVP in amorphous solid dispersions. The clean suppression of the nifedipine signal in a physically mixed sample, and later equilibration in a 95:5 mixture of PVP and 13 C-enriched nifedipine, as well as near-equilibration after spin diffusion starting from nifedipine and 12 C confirms that the experiment works correctly. 20- μ s or 25- μ s 1 H 12 filtering selectively suppresses or inverts magnetization in PVP, respectively, while 2-ms $T_{1\rho H}$ filtering selectively suppresses magnetization of bound 12 C. Then, spin diffusion from nifedipine to PVP can occur. In high-Nif samples, significant spin diffusion from nifedipine to PVP is observed within 12 S ms, but does not reach complete equilibrium even after 100 ms, which indicates that Nifedipine and PVP are not homogeneously mixed. With partial inversion of the PVP magnetization, the nonequilibration is even more pronounced. Lack of equilibration has also been observed by 1 H- 13 C HETCOR NMR with 1 H spin diffusion. Inhomogeneous mixing has further been confirmed by differential T_{1H} relaxation in 1 H inversion recovery, and the observation of 1 C-nm domains in AFM imaging. Incomplete equilibration during spin diffusion and T_{1H} relaxation was simulated in a two-mixed-phases model, which yielded constraints on the compositions of the two mixed phases. These results have demonstrated that our spin-diffusion NMR method together with

relaxation measurements can successfully quantify phase separation and compositions of ASDs prepared by spray drying and hot-melt extrusion.

5. Acknowledgments

The authors appreciate Prof. Lynne S. Taylor (Department of Industrial and Physical Pharmacy, College of Pharmacy, Purdue University, West Lafayette, Indiana, USA) for her insightful discussions on possible scenarios of miscibility and homogeneity. Funding support by Merck Sharp & Dohme Corp., a subsidiary of Merck & Co., Inc, is gratefully acknowledged. The solid-state NMR spectrometer used in this work was funded by the NSF MRI program (Award No. 1726346).

6. References

- (1) Amidon, G. L.; Lennernäs, H.; Shah, V. P.; Crison, J. R. A Theoretical Basis for a Biopharmaceutic Drug Classification: The Correlation of in Vitro Drug Product Dissolution and in Vivo Bioavailability. *Pharm. Res.* **1995**, *12*, (3), 413-420.
- (2) Loftsson, T.; Brewster, M. E. Pharmaceutical applications of cyclodextrins: basic science and product development. *J. Pharm. Pharmacol.* **2010**, *62*, (11), 1607-1621.
- (3) Van den Mooter, G. The use of amorphous solid dispersions: A formulation strategy to overcome poor solubility and dissolution rate. *Drug Discov*. *Today* **2012**, *9*, (2), e79-e85.
- (4) Sekiguchi, K.; Obi, N.; Ueda, Y. Studies on Absorption of Eutectic Mixture. Ii. Absorption of Fused Conglomerates of Chloramphenicol and Urea in Rabbits. *Chem Pharm Bull (Tokyo)* **1964**, *12*, 134-144.
- (5) Tao, J.; Sun, Y.; Zhang, G. G.; Yu, L. Solubility of small-molecule crystals in polymers: D-mannitol in PVP, indomethacin in PVP/VA, and nifedipine in PVP/VA. *Pharm Res* **2009**, *26*, (4), 855-864.
- (6) Chiou, W. L.; Riegelman, S. Pharmaceutical applications of solid dispersion systems. *J. Pharm. Sci.* **1971**, *60*, (9), 1281-1302.
- (7) LaFountaine, J. S.; McGinity, J. W.; Williams, R. O. Challenges and Strategies in Thermal Processing of Amorphous Solid Dispersions: A Review. *Aaps Pharmscitech* **2016**, *17*, (1), 43-55.
- (8) Marsac, P. J.; Shamblin, S. L.; Taylor, L. S. Theoretical and Practical Approaches for Prediction of Drug-Polymer Miscibility and Solubility. *Pharm. Res.* **2006**, *23*, (10), 2417.
- (9) Marsac, P. J.; Li, T.; Taylor, L. S. Estimation of drug-polymer miscibility and solubility in amorphous solid dispersions using experimentally determined interaction parameters. *Pharm Res* **2009**, *26*, (1), 139-151.
- (10) Qian, F.; Huang, J.; Hussain, M. A. Drug–polymer solubility and miscibility: Stability consideration and practical challenges in amorphous solid dispersion development. *J. Pharm. Sci.* **2010**, *99*, (7), 2941-2947.

- (11) Marsac, P. J.; Rumondor, A. C.; Nivens, D. E.; Kestur, U. S.; Stanciu, L.; Taylor, L. S. Effect of temperature and moisture on the miscibility of amorphous dispersions of felodipine and poly(vinyl pyrrolidone). *J Pharm Sci* **2010**, *99*, (1), 169-185.
- (12) Anderson, B. D. Predicting Solubility/Miscibility in Amorphous Dispersions: It Is Time to Move Beyond Regular Solution Theories. *J Pharm Sci-Us* **2018**, *107*, (1), 24-33.
- (13) Duggirala, N. K.; Li, J.; Kumar, N. S. K.; Gopinath, T.; Suryanarayanan, R. A supramolecular synthon approach to design amorphous solid dispersions with exceptional physical stability. *Chem Commun (Camb)* **2019**, *55*, (39), 5551-5554.
- (14) Kothari, K.; Ragoonanan, V.; Suryanarayanan, R. The role of polymer concentration on the molecular mobility and physical stability of nifedipine solid dispersions. *Mol Pharm* **2015**, *12*, (5), 1477-1484.
- (15) Li, Y.; Yu, J.; Hu, S.; Chen, Z.; Sacchetti, M.; Sun, C. C.; Yu, L. Polymer Nanocoating of Amorphous Drugs for Improving Stability, Dissolution, Powder Flow, and Tabletability: The Case of Chitosan-Coated Indomethacin. *Mol Pharm* **2019**, *16*, (3), 1305-1311.
- (16) Ueda, K.; Taylor, L. S. Polymer Type Impacts Amorphous Solubility and Drug-Rich Phase Colloidal Stability: A Mechanistic Study Using Nuclear Magnetic Resonance Spectroscopy. *Mol Pharm* **2020**, *17*, (4), 1352-1362.
- (17) Saboo, S.; Mugheirbi, N. A.; Zemlyanov, D. Y.; Kestur, U. S.; Taylor, L. S. Congruent release of drug and polymer: A "sweet spot" in the dissolution of amorphous solid dispersions. *J Control Release* **2019**, 298, 68-82.
- (18) Mehta, M.; Kothari, K.; Ragoonanan, V.; Suryanarayanan, R. Effect of Water on Molecular Mobility and Physical Stability of Amorphous Pharmaceuticals. *Mol Pharm* **2016**, *13*, (4), 1339-1346.
- (19) Li, N.; Gilpin, C. J.; Taylor, L. S. Understanding the Impact of Water on the Miscibility and Microstructure of Amorphous Solid Dispersions: An AFM-LCR and TEM-EDX Study. *Mol Pharm* **2017**, *14*, (5), 1691-1705.
- (20) Van Eerdenbrugh, B.; Lo, M.; Kjoller, K.; Marcott, C.; Taylor, L. S. Nanoscale mid-infrared evaluation of the miscibility behavior of blends of dextran or maltodextrin with poly(vinylpyrrolidone). *Mol Pharm* **2012**, *9*, (5), 1459-1469.
- (21) Purohit, H. S.; Taylor, L. S. Miscibility of Itraconazole-Hydroxypropyl Methylcellulose Blends: Insights with High Resolution Analytical Methodologies. *Mol Pharmaceut* **2015**, *12*, (12), 4542-4553.
- (22) Meng, F.; Dave, V.; Chauhan, H. Qualitative and quantitative methods to determine miscibility in amorphous drug-polymer systems. *Eur J Pharm Sci* **2015**, *77*, 106-111.
- (23) Rumondor, A. C.; Ivanisevic, I.; Bates, S.; Alonzo, D. E.; Taylor, L. S. Evaluation of drug-polymer miscibility in amorphous solid dispersion systems. *Pharm Res* **2009**, *26*, (11), 2523-2534.

- (24) Keratichewanun, S.; Yoshihashi, Y.; Sutanthavibul, N.; Terada, K.; Chatchawalsaisin, J. An Investigation of Nifedipine Miscibility in Solid Dispersions Using Raman Spectroscopy. *Pharm Res* **2015**, *32*, (7), 2458-2473.
- (25) Purohit, H. S.; Ormes, J. D.; Saboo, S.; Su, Y. C.; Lamm, M. S.; Mann, A. K. P.; Taylor, L. S. Insights into Nano- and Micron-Scale Phase Separation in Amorphous Solid Dispersions Using Fluorescence-Based Techniques in Combination with Solid State Nuclear Magnetic Resonance Spectroscopy. *Pharm Res-Dordr* 2017, 34, (7), 1364-1377.
- (26) Lamm, M. S.; DiNunzio, J.; Khawaja, N. N.; Crocker, L. S.; Pecora, A. Assessing Mixing Quality of a Copovidone-TPGS Hot Melt Extrusion Process with Atomic Force Microscopy and Differential Scanning Calorimetry. *Aaps Pharmscitech* **2016**, *17*, (1), 89-98.
- (27) Krause, S.; Iskandar, M. In *Polymer Alloys: Blends, Blocks, Grafts, and Interpenetrating Networks*, Klempner, D.; Frisch, K. C., Eds.; Springer US: Boston, MA, 1977, pp 231-243.
- (28) Purohit, H. S.; Ormes, J. D.; Saboo, S.; Su, Y.; Lamm, M. S.; Mann, A. K. P.; Taylor, L. S. Insights into Nano- and Micron-Scale Phase Separation in Amorphous Solid Dispersions Using Fluorescence-Based Techniques in Combination with Solid State Nuclear Magnetic Resonance Spectroscopy. *Pharm. Res.* **2017**, *34*, (7), 1364-1377.
- (29) Hanada, M.; Jermain, S. V.; Lu, X. Y.; Su, Y. C.; Williams, R. O. Predicting physical stability of ternary amorphous solid dispersions using specific mechanical energy in a hot melt extrusion process. *Int J Pharmaceut* **2018**, *548*, (1), 571-585.
- (30) Li, N.; Taylor, L. S. Nanoscale Infrared, Thermal, and Mechanical Characterization of Telaprevir-Polymer Miscibility in Amorphous Solid Dispersions Prepared by Solvent Evaporation. *Mol Pharmaceut* **2016**, *13*, (3), 1123-1136.
- (31) Li, N.; Taylor, L. S. Microstructure Formation for Improved Dissolution Performance of Lopinavir Amorphous Solid Dispersions. *Mol Pharmaceut* **2019**, *16*, (4), 1751-1765.
- (32) Tian, B.; Tang, X.; Taylor, L. S. Investigating the Correlation between Miscibility and Physical Stability of Amorphous Solid Dispersions Using Fluorescence-Based Techniques. *Mol Pharm* **2016**, *13*, (11), 3988-4000.
- (33) Clauss, J.; Schmidt-Rohr, K.; Spiess, H. W. Determination of domain sizes in heterogeneous polymers by solid-state NMR. *Acta Polym.* **1993**, *44*, (1), 1-17.
- (34) Wu, R. R.; Kao, H. M.; Chiang, J. C.; Woo, E. M. Solid-state NMR studies on phase behavior and motional mobility in binary blends of polystyrene and poly(cyclohexyl methacrylate). *Polymer* **2002**, *43*, (1), 171-176.
- (35) Lowinger, M. B.; Su, Y. C.; Lu, X. Y.; Williams, R. O.; Zhang, F. Can drug release rate from implants be tailored using poly(urethane) mixtures? *Int J Pharmaceut* **2019**, *557*, 390-401.
- (36) Yuan, X.; Sperger, D.; Munson, E. J. Investigating Miscibility and Molecular Mobility of Nifedipine-PVP Amorphous Solid Dispersions Using Solid-State NMR Spectroscopy. *Mol. Pharmaceutics* **2014**, *11*, (1), 329-337.

- (37) Pham, T. N.; Watson, S. A.; Edwards, A. J.; Chavda, M.; Clawson, J. S.; Strohmeier, M.; Vogt, F. G. Analysis of Amorphous Solid Dispersions Using 2D Solid-State NMR and H-1 T-1 Relaxation Measurements. *Mol Pharmaceut* **2010**, *7*, (5), 1667-1691.
- (38) Mu, D.; Li, J. Q.; Zhou, Y. H. Modeling and analysis of the compatibility of polystyrene/poly(methyl methacrylate) blends with four inducing effects. *J Mol Model* **2011**, *17*, (3), 607-619.
- (39) P., C.; P., N.; R., E. R. Characterization of heterogeneous polymer blends by two-dimensional proton spin diffusion spectroscopy. *Macromolecules* **1985**, *18*, (1), 119-122.
- (40) Spiegel, S.; Schmidt-Rohr, K.; Boeffel, C.; Spiess, H. W. H-1 Spin-Diffusion Coefficients of Highly Mobile Polymers. *Polymer* **1993**, *34*, (21), 4566-4569.
- (41) Duan, P.; Moreton, J. C.; Tavares, S. R.; Semino, R.; Maurin, G.; Cohen, S. M.; Schmidt-Rohr, K. Polymer Infiltration into Metal-Organic Frameworks in Mixed-Matrix Membranes Detected in Situ by NMR. *J Am Chem Soc* **2019**, *141*, (18), 7589-7595.
- (42) Duan, P.; Li, X.; Wang, T.; Chen, B.; Juhl, S. J.; Koeplinger, D.; Crespi, V. H.; Badding, J. V.; Schmidt-Rohr, K. The Chemical Structure of Carbon Nanothreads Analyzed by Advanced Solid-State NMR. *J Am Chem Soc* **2018**, *140*, (24), 7658-7666.
- (43) Su, Y. C.; Waring, A. J.; Ruchala, P.; Hong, M. Structures of beta-Hairpin Antimicrobial Protegrin Peptides in Lipopolysaccharide Membranes: Mechanism of Gram Selectivity Obtained from Solid-State Nuclear Magnetic Resonance. *Biochemistry-Us* **2011**, *50*, (12), 2072-2083.
- (44) Aso, Y.; Yoshioka, S.; Miyazaki, T.; Kawanishi, T.; Tanaka, K.; Kitamura, S.; Takakura, A.; Hayashi, T.; Muranushi, N. Miscibility of nifedipine and hydrophilic polymers as measured by H-1-NMR spin-lattice relaxation. *Chem Pharm Bull* **2007**, *55*, (8), 1227-1231.
- (45) Ma, X.; Huang, S.; Lowinger, M. B.; Liu, X.; Lu, X.; Su, Y.; Williams, R. O., 3rd. Influence of mechanical and thermal energy on nifedipine amorphous solid dispersions prepared by hot melt extrusion: Preparation and physical stability. *Int J Pharm* **2019**, *561*, 324-334.
- (46) Yang, F.; Su, Y.; Zhang, J.; DiNunzio, J.; Leone, A.; Huang, C.; Brown, C. D. Rheology Guided Rational Selection of Processing Temperature To Prepare Copovidone-Nifedipine Amorphous Solid Dispersions via Hot Melt Extrusion (HME). *Mol Pharm* **2016**, *13*, (10), 3494-3505.
- (47) Coleman, G. B.; Andrews, H. C. Image segmentation by clustering. *Proceedings of the IEEE* **1979**, *67*, (5), 773-785.
- (48) Pedregosa, F.; Varoquaux, G.; Gramfort, A.; Michel, V.; Thirion, B.; Grisel, O.; Blondel, M.; Prettenhofer, P.; Weiss, R.; Dubourg, V.; Vanderplas, J.; Passos, A.; Cournapeau, D.; Brucher, M.; Perrot, M.; Duchesnay, É. Scikit-learn: Machine Learning in Python. *Journal of Machine Learning Research* **2011**, *12*, 2825-2830.
- (49) Chen, Q.; Hou, S. S.; Schmidt-Rohr, K. A simple scheme for probehead background suppression in one-pulse ¹H NMR. *Solid State Nucl. Magn. Reson.* **2004**, *26*, (1), 11-15.

- (50) Pines, A.; Gibby, M. G.; Waugh, J. S. Proton-enhanced NMR of dilute spins in solids. *J. Chem. Phys.* **1973**, *59*, (2), 569-590.
- (51) Schaefer, J.; Stejskal, E. O. Carbon-13 nuclear magnetic resonance of polymers spinning at the magic angle. *J. Am. Chem. Soc.* **1976**, *98*, (4), 1031-1032.
- (52) van Rossum, B. J.; Förster, H.; de Groot, H. J. M. High-Field and High-Speed CP-MAS13C NMR Heteronuclear Dipolar-Correlation Spectroscopy of Solids with Frequency-Switched Lee–Goldburg Homonuclear Decoupling. *J. Magn. Reson.* **1997**, *124*, (2), 516-519.
- (53) Schmidt-Rohr, K.; Spiess, H. W. *Multidimensional Solid-State NMR and Polymers*; Academic Press: San Diego, 1994.
- (54) Chen, Q.; Schmidt-Rohr, K. Measurement of the local 1H spin-diffusion coefficient in polymers. *Solid State Nucl. Magn. Reson.* **2006**, *29*, (1–3), 142-152.
- (55) Lu, X.; Huang, C.; Lowinger, M. B.; Yang, F.; Xu, W.; Brown, C. D.; Hesk, D.; Koynov, A.; Schenck, L.; Su, Y. Molecular Interactions in Posaconazole Amorphous Solid Dispersions from Two-Dimensional Solid-State NMR Spectroscopy. *Mol Pharm* **2019**, *16*, (6), 2579-2589.
- (56) Kawakami, K.; Harada, T.; Miura, K.; Yoshihashi, Y.; Yonemochi, E.; Terada, K.; Moriyama, H. Relationship between crystallization tendencies during cooling from melt and isothermal storage: toward a general understanding of physical stability of pharmaceutical glasses. *Mol Pharm* **2014**, *11*, (6), 1835-1843.
- (57) Hancock, B. C.; Shamblin, S. L.; Zografi, G. Molecular mobility of amorphous pharmaceutical solids below their glass transition temperatures. *Pharm Res* **1995**, *12*, (6), 799-806.
- (58) Yoshioka, M.; Hancock, B. C.; Zografi, G. Crystallization of indomethacin from the amorphous state below and above its glass transition temperature. *J Pharm Sci* **1994**, *83*, (12), 1700-1705.
- (59) Anderson, B. D. Predicting Solubility/Miscibility in Amorphous Dispersions: It Is Time to Move Beyond Regular Solution Theories. *J Pharm Sci* **2018**, *107*, (1), 24-33.
- (60) DeBoyace, K.; Wildfong, P. L. D. The Application of Modeling and Prediction to the Formation and Stability of Amorphous Solid Dispersions. *J Pharm Sci* **2018**, *107*, (1), 57-74.
- (61) Aso Y; Yoshioka S; S, K. Relationship between the crystallization rates of amorphous nifedipine, phenobarbital, and flopropione, and their molecular mobility as measured by their enthalpy relaxation and (1)H NMR relaxation times. *J Pharm Sci* **2000**, 89, (3), 408-416.
- (62) Aso, Y.; Yoshioka, S. Molecular mobility of nifedipine–PVP and phenobarbital–PVP solid dispersions as measured by 13C-NMR spin-lattice relaxation time. *J. Pharm. Sci.* **2006**, *95*, (2), 318-325.
- (63) Brettmann, B.; Bell, E.; Myerson, A.; Trout, B. Solid-State NMR Characterization of High-Loading Solid Solutions of API and Excipients Formed by Electrospinning. *J. Pharm. Sci.* **2012**, *101*, (4), 1538-1545.

- (64) Sarpal, K.; Delaney, S.; Zhang, G. G. Z.; Munson, E. J. Phase Behavior of Amorphous Solid Dispersions of Felodipine: Homogeneity and Drug-Polymer Interactions. *Mol Pharm* **2019**, *16*, (12), 4836-4851.
- (65) C., S.; M., G. Theory of nucleation and growth during phase separation. *Phys Rev E.* **1999**, 59, (4), 4175-4187.